Spectroscopic investigation of complex nuclear excitations in ^{66}Ga

U. S. Ghosh,[1] S. Rai,[1,*] B. Mukherjee,[1,†] A. Biswas,[1] A. K. Mondal,[1] K. Mandal,[1] A. Chakraborty,[1] S. Chakraborty,[2,‡] G. Mukherjee,[3] A. Sharma,[4] I. Bala,[5] S. Muralithar,[5] and R. P. Singh[5]

[1]*Department of Physics, Siksha-Bhavana, Visva-Bharati, Santiniketan, West Bengal 731235, India*
[2]*Department of Physics, Institute of Science, Banaras Hindu University, Varanasi 221005, India*
[3]*Variable Energy Cyclotron Centre, 1/AF Bidhannagar, Kolkata 700064, India*
[4]*Department of Physics, Himachal Pradesh University, Shimla 171005, India*
[5]*Inter University Accelerator Centre (IUAC), Aruna Asaf Ali Marg, New Delhi 110067, India*

(Received 23 November 2019; revised 5 July 2020; accepted 29 July 2020; published 24 August 2020)

In-beam spectroscopic technique using the fusion evaporation reaction ^{52}Cr(^{18}O, $1p3n$), at a beam energy of 72.5 MeV, was employed to explore the structural phenomena in ^{66}Ga, mainly at intermediate and high spins. The experimental setup involved an array of 14 Compton suppressed Ge clover detectors, placed around the target position to detect emitted γ rays from excited states. A new level scheme has been proposed, which is enriched with more than 20 new transitions and is extended up to an excitation energy $\approx$12 MeV. A few observed intermediate spin states of ^{66}Ga are discussed in the framework of coupling of single-particle configurations with the vibrational core of ^{64}Zn. Shell model calculations have also been performed with two different interactions, viz., jj44bpn and jun45pn, for the interpretation of the observed level structure in ^{66}Ga.

DOI: 10.1103/PhysRevC.102.024328

I. INTRODUCTION

Complex excitations, including single-particle and collective ones, have been observed in Zn [1–8], Ga [9–12], and Ge [13,14] isotopes, manifesting various shapes, which are explained by simple theoretical models like the shell model, the interacting Boson model, and cranked Nilsson Strutinsky calculations. Nuclear level structures in ^{65,67}Ga are explained in the framework of the interacting boson-fermion plus broken pair model (IBFBPM), where low and medium spin negative parity yrast states are explained as originating from the coupling of one quasiproton of the negative parity $1f$ or $2p$ orbital with the multiphonon vibrational states of ^{64}Zn and ^{66}Zn, respectively. High spin states in the former two nuclei are mainly of three-quasiparticle nature, originating from coupling of one proton with a broken neutron pair excitations. A similar study on ^{63}Ga and ^{65}Ga by Weiszflog *et al.* [9] revealed rotational-like structures built on $9/2^+$ and $19/2^{(-)}$ states in both nuclei. Angular momenta of the rotational states, built on the $9/2^+$ states, were reported to be generated from the alignment of a neutron pair in the $g_{9/2}$ orbital. As the $g_{9/2}$ orbital is occupied by a single proton, proton crossing is blocked by the Pauli exclusion principle. All the observations in ^{63,65,67}Ga suggest that a large variety of phenomena emerge out of the competition between single-particle and collective excitations, consisting of both vibrational and rotational degrees of freedom. Interestingly, in ^{68}Ga, high spin states, viz., 9^+, 11^+, 13^+, were compared respectively with $9/2^+$, $13/2^+$, $17/2^+$ energy states of ^{67}Ga by Singh *et al.* [12]. Configurations of these states in ^{67}Ga were stated to be built predominantly from one $\pi g_{9/2}$ quasiproton plus phonon configuration coming from the vibrational core of ^{66}Zn. Alternatively, it can be understood that 11^+ and 13^+ states of ^{68}Ga originate from the couplings of 9^+ ($\pi g_{9/2} \otimes \nu g_{9/2}$) state of ^{68}Ga with multiphonon vibrational states of ^{66}Zn.

In order to understand how this coupling of phonons with single particles qualifies to yield the measured energy values, we have compared some already existing data with the coupling configurations. Intermediate spin states of ^{63,65,67}Ga, viz., $13/2^+$, $17/2^+$ and $21/2^+$ [9,11], are compared with $2_1^+ \otimes 9/2^+$, $4_1^+ \otimes 9/2^+$ and $6_1^+ \otimes 9/2^+$ coupled states, respectively, in Fig. 1. As is evident from the figure, observed states $13/2^+$, $17/2^+$, and $21/2^+$ of ^{63}Ga are very close in energy respectively to those states originating from couplings of 2_1^+, 4_1^+, and 6_1^+ core states of ^{62}Zn [4] with the $9/2^+$ state of ^{63}Ga. Similarly, in the case of ^{65}Ga and ^{67}Ga, core states are the multiphonon vibrational states of ^{64}Zn [7] and ^{66}Zn [15], respectively. In the case of ^{65}Ga, good agreement is observed for $13/2^+$ and $17/2^+$ states but some discrepancy appears at $21/2^+$, whereas in ^{67}Ga only the $13/2^+$ state is in close proximity to the core-coupled state. This could be due to the significant contribution arising from residual interaction between the core and the particle with increasing spin and mass number.

So, situated in between ^{65}Ga and ^{67}Ga, ^{66}Ga is expected to have a similar kind of systematics and intermediate spin states will have complex structures, with contributions from

*Presently at Department of Physics, Salesian College, Siliguri Campus, Siliguri 734001, India.
†buddhadev.mukherjee@visva-bharati.ac.in
‡Presently at IUAC, New Delhi, India.

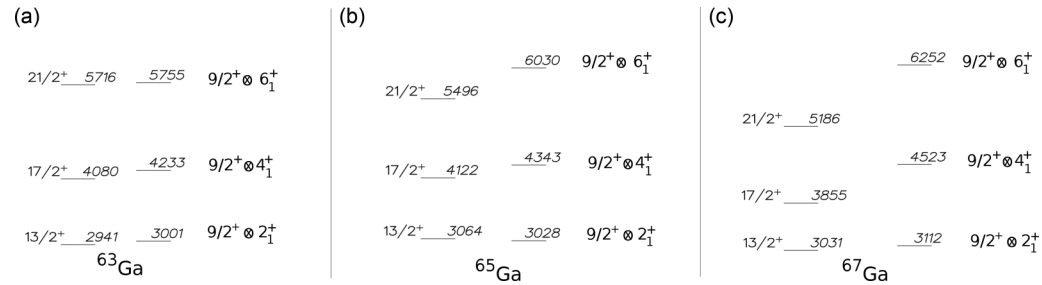

FIG. 1. (a) Energy values of the observed $13/2^+$, $17/2^+$ and $21/2^+$ states in ^{63}Ga (data taken from Ref. [9]) are compared with the sum energy values of $9/2^+$ state (of ^{63}Ga) coupled to, respectively, 2^+_1, 4^+_1, and 6^+_1 vibrational states of ^{62}Zn [4] forming, respectively, coupled states $13/2^+$, $17/2^+$, and $21/2^+$ in ^{63}Ga. Here, energy values are quoted in keV. (b) Same as panel (a) but for ^{65}Ga, which has core states originating from ^{64}Zn [7] and $9/2^+$, $13/2^+$, $17/2^+$ and $21/2^+$ states from ^{65}Ga [9,11]. (c) Same as panel (a) but for ^{67}Ga, which has core states originating from ^{66}Zn [15] and $9/2^+$, $13/2^+$, $17/2^+$ and $21/2^+$ states of ^{67}Ga [11]. Please see text for details.

both single-particle and collective excitations. This kind of investigation on observed levels in ^{66,68}Ga has been performed and is described later in detail in the discussion section.

Earlier studies on ^{66}Ga were done with modest detector setups using electron-capture decay and reactions like ^{64}Zn$(\alpha, pn\gamma)$, ^{63}Cu$(\alpha, n\gamma)$, ^{64}Zn(α, d), ^{66}Zn$(p, n\gamma)$, ^{66}Zn$(^3$He$, t)$, and ^{56}Fe$(^{13}$C$, p2n\gamma)$, which were used to explore only low and medium spin states [16–23]. The most recent study by Bhattacharjee *et al.*, [10] was performed using 15 Compton suppressed Ge clover detectors; the level scheme was extended up to $21^{(+)}$. Two bandlike structures were observed, with the positive and negative parity bands being described to have originated from $\nu(g_{9/2})^3(f_{5/2})^2 \otimes \pi(g_{9/2})^1(f_{5/2})^2$ and $\nu(g_{9/2})^2(f_{5/2})^1 \otimes \pi(g_{9/2})^1(f_{5/2})^2$ configurations, respectively. As in ^{63,65}Ga and ^{65}Zn, the role of the $g_{9/2}$ neutron pair appears to be very significant in ^{66}Ga, as its alignment along the rotational axis generates the angular momenta of the high spin states in the bands. Here, we report on an experimental investigation on medium and high spin excitations of ^{66}Ga as well as its shell model description mainly at low and intermediate spin values.

II. EXPERIMENTAL DETAILS AND DATA ANALYSIS

In the fusion-evaporation reaction, an ^{18}O beam at 72.5 MeV was obtained from the 15-UD pelletron accelerator [24] at the Inter University Accelerator Centre (IUAC), New Delhi. An isotope of ^{52}Cr of thickness 1 mg/cm^2 (isotopic abundance ≈99%), backed by 7 mg/cm^2 gold, was used as target. The emitted γ rays were detected in coincidence with 14 Compton suppressed high-purity germanium (HPGe) clover detectors of the Indian National Gamma Array (INGA) [25]. Detectors were placed at three different angles, viz., 123°, 148°, and 90° with respect to the beam direction. Time-stamped data were collected in list mode with the help of the computer-aided measurement and control (CAMAC) based data acquisition software CANDLE [26]. Different symmetric and angle dependent E_γ-E_γ matrices from coincidence data were constructed using analysis packages, viz., RADWARE [27] and INGASORT [28]. More details about the target, experimental setup, and data analysis procedure can be found in Refs. [5,29]. Multipolarity of a transition was determined from the DCO ratio (R_{DCO}) [30], which in the present INGA geometry is defined as

$$R_{DCO} = \frac{I_{\gamma_1} \text{ at } 148^\circ \text{ gated by } \gamma_2 \text{ at } 90^\circ}{I_{\gamma_1} \text{ at } 90^\circ \text{ gated by } \gamma_2 \text{ at } 148^\circ},$$

where I_{γ_1} is the measured intensity of γ_1 when the gating transition is γ_2. The expected R_{DCO} values for the stretched quadrupole and the dipole transitions are ≈1.0 (2.0) and ≈0.5 (1.0), for pure quadrupole (dipole) gates respectively. In this work, R_{DCO} values are measured by using stretched $E2$ gates of 1189 ($9^+_1 \rightarrow 7^+_1$), 1268 ($9^+_2 \rightarrow 7^+_2$), 947 ($13^+_1 \rightarrow 11^+_1$), 1058 ($15^+ \rightarrow 13^+_2$), and 1002 keV ($14^-_1 \rightarrow 12^-_3$) of ^{66}Ga. Electric or magnetic nature of γ-ray transitions was determined from the polarization measurement [31,32], which was analyzed by constructing two asymmetric matrices, one with perpendicular and the other with parallel scattered events (i.e., the events with γ rays scattered perpendicular or parallel to the emission plane) of 90° detectors in one axis and corresponding γ rays detected at all angles on another axis. The asymmetry parameter was calculated as

$$\Delta_{\text{asym}} = \frac{a(E_\gamma)N_\perp - N_\parallel}{a(E_\gamma)N_\perp + N_\parallel},$$

where $a(E_\gamma)$ represents the experimental asymmetry correction factor for clover detectors at 90° of the present INGA setup and was determined from the ratio of the parallel ($N_\parallel$) and the perpendicular ($N_\perp$) scattered events obtained from an unpolarized source. It is defined as

$$a(E_\gamma) = \frac{N_\parallel(\text{unpolarized})}{N_\perp(\text{unpolarized})}.$$

The value of the asymmetry correction factor for the present detector setup is found to be ≈1.03(2) in the energy range ≈0.1–1.5 MeV using the standard ^{152}Eu radioactive source. Electric (magnetic) type transitions will have positive (negative) polarization asymmetry (Δ_{asym}) value, while a near zero value of Δ_{asym} indicates that there is a strong admixture. Figures 2 and 3 represent, respectively, the plots of R_{DCO} and polarization asymmetry values for different transitions belonging to ^{66}Ga, which were observed in the measurements.

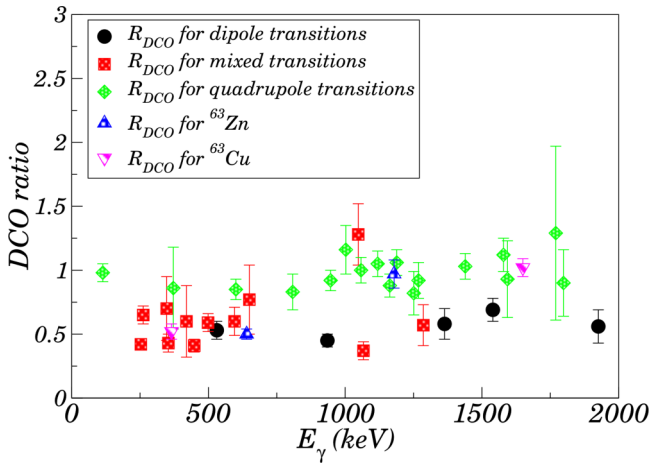

FIG. 2. R_{DCO} values for different transitions of ^{66}Ga (gated by different $E2$ transitions as mentioned in the text and in Table I) along with those of selected transitions having definite multipolarities, viz., of ^{63}Cu (E_γ = 365 and 1650 keV respectively, for $7/2^- \rightarrow 5/2^-$ and $13/2^+ \rightarrow 9/2^+$ transitions) and ^{63}Zn (E_γ = 640 and 1179 keV respectively, for $9/2^+ \rightarrow 7/2^-$ and $17/2^+ \rightarrow 13/2^+$ transitions), populated in the fusion evaporation reaction. The latter four transitions are used to fix the reference values in the current analysis and to validate the same. For ^{63}Cu and ^{63}Zn the gating transitions are 342 ($17/2^+ \rightarrow 13/2^+$) and 882 keV ($13/2^+ \rightarrow 9/2^+$) stretched $E2$ type, respectively.

III. RESULTS AND DISCUSSION

A new level scheme of ^{66}Ga (Fig. 4) has been proposed in the present work, which is based on the coincidence relationship, relative intensity balance, angular correlation, and polarization measurements of the emitted γ rays. Almost all the transitions reported previously are observed in this measurement. New transitions are marked with asterisks in the level scheme. A total of 21 new transitions and 20 new

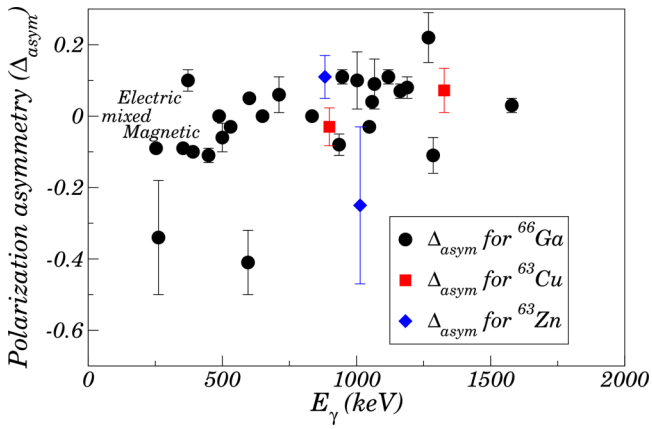

FIG. 3. Polarization asymmetry values ($\Delta_{\rm asym}$) for different transitions in ^{66}Ga, measured in the present experiment. Here, the asymmetry values of 1013 keV ($7/2^- \rightarrow 5/2^-$) and 882 keV ($13/2^+ \rightarrow 9/2^+$) transitions of ^{63}Zn and 899 ($7/2^- \rightarrow 5/2^-$) and 1327 keV ($7/2^- \rightarrow 3/2^-$) transitions of ^{63}Cu are also plotted for the same purpose as in the DCO plot (Fig. 2).

levels have been placed in the level scheme. Transitions which are in coincidence are shown in the typical gated spectra (Fig. 5). Here, the gated spectra are generated through a "logical AND" of the two single gates, which is a feature available in RADWARE.

The 44 ($1^+ \rightarrow 0^+$) and 22 keV ($2^+ \rightarrow 1^+$) γ-ray transitions, which decay respectively from the 44 ($I^\pi = 1^+$) and 66 keV ($I^\pi = 2^+$) states, as were reported previously [16,17], are not observed in the present work as the energies are below the measured energy threshold of the γ-ray spectrometer, we used. So, the ground 0^+ state is not shown in the new level scheme. Najam *et al.* [20] argue, in part, for a spin of 2 for the state at 66 keV based on the absence of feeding from a 0^+ parent in electron-capture decay, as noted by de Boer *et al.* [33]. Morand *et al.* [17] subsequently considered the argument strengthened somewhat based on lifetime measurements made in other works that suggested that the 22 and 44 keV γ rays are $M1$ in nature, and thus that the 2^+ assignment is firm. There is a conflict between those authors and Evaluated Nuclear Structure Data File (ENSDF) evaluators regarding this firm 2^+ spin-parity assignment. However, lifetimes likely do not adequately distinguish between $1^+ \rightarrow 1^+$ and $2^+ \rightarrow 1^+$ $M1$ transitions. So, these are probably considered to be weak arguments by ENSDF evaluators and they also continue to show the state at 66 keV as $(2)^+$. To keep things simple in this work, we have followed the assignment of Refs. [20] and [17], and multipolarities of the higher spin states are determined based on this assignment.

In this work the DCO ratios of many transitions are determined using 1189 keV ($9^+ \rightarrow 7^+$) $E2$ gate. Multipolarity of the 1189 keV γ ray is adopted from the literature [10]. Determination of multipolarity of all the transitions (as given in Table I) was not possible using a single gate, so other transitions, which are stretched quadrupole in the 1189 keV $E2$ gate, are used for this purpose.

Here, the states with energies 863, 414, and 162 keV decay in cascade respectively by strong 448, 253, and 96 keV γ rays to the 2^+ state at 66 keV. The measured value of the DCO ratio (R_{DCO}) of 96 keV, and also the measured R_{DCO} and polarization asymmetry ($\Delta_{\rm asym}$) of 253 and 448 keV γ rays suggest 3^+, 4^+, and 5^+ spin-parity assignments for 162, 414, and 863 keV states respectively. Measured R_{DCO} and $\Delta_{\rm asym}$ of 834 and 935 keV transitions suggest a 5^+ spin-parity assignment for the 1350 keV state.

Figure 5(a) indicates that the height of the 834 keV peak is about one third of that of 935 keV peak. These transitions decay from the 1350 keV level and have been found to be present in the spectrum gated on 1189 and 1540 keV transitions that feed the 1350 keV level. However, the measured intensity of the 935 keV transition indicates that the size of this transition is significantly larger in the table than is seen in the figure. This anomaly in branching is suggestive of the possible presence of a weak doublet 834 keV transition which could neither be properly identified nor be placed in the level scheme due to the lack of sufficient statistics.

The state at 516 keV is assigned with a spin-parity 4^+, depending upon the measured R_{DCO} and $\Delta_{\rm asym}$ of the depopulating 354 keV γ ray. The state at 1463 keV decays to that at 863 keV (5^+) by a strong 601 keV γ-ray transition. Measured

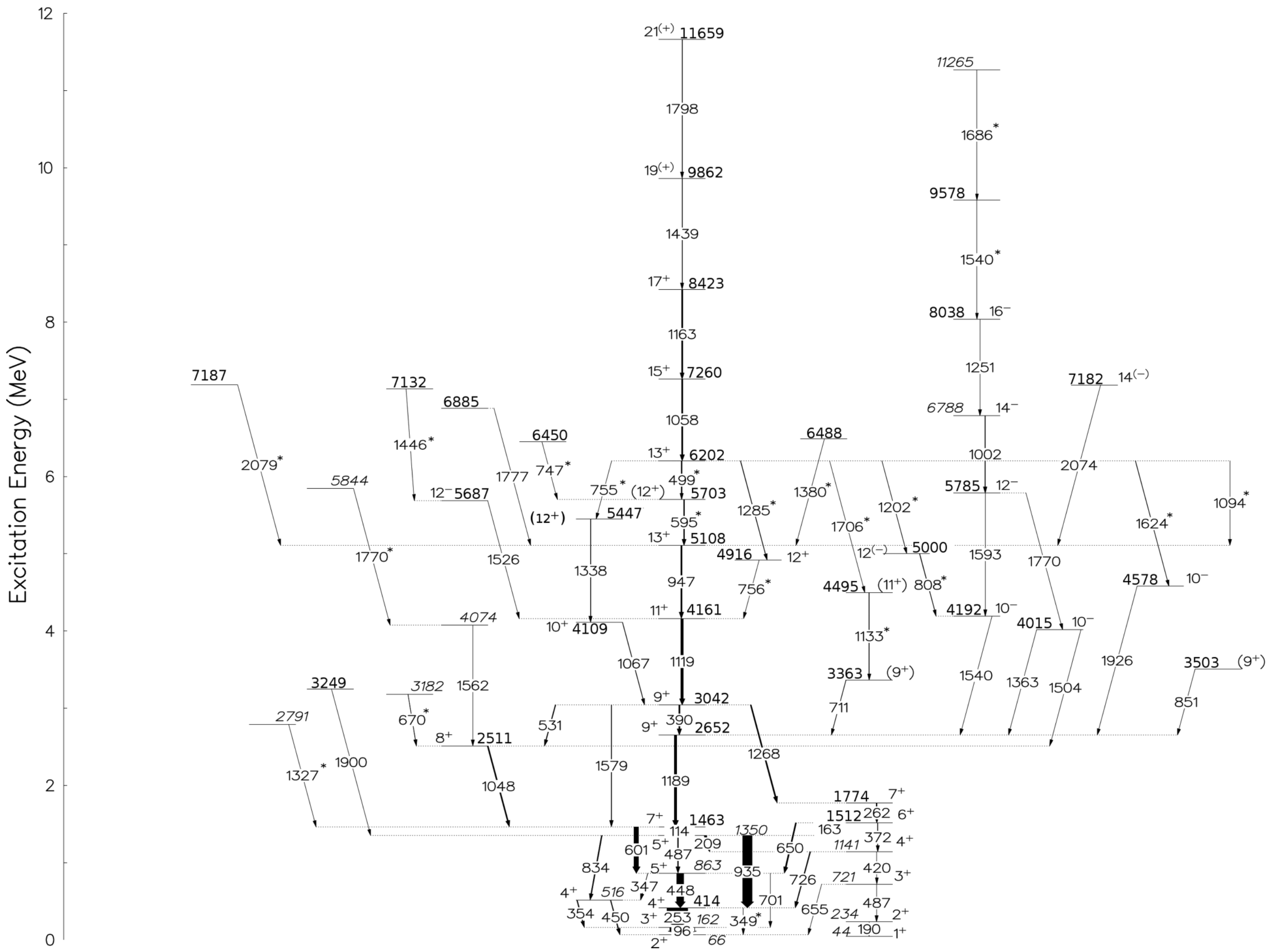

FIG. 4. Proposed level scheme of ^{66}Ga. Widths of the arrows are proportional to the relative intensity of the respective transition observed in the present experiment. New transitions are marked with asterisks. The energies in the figure are in keV.

R_{DCO} and $\Delta_{\rm asym}$ of the 601 keV transition suggest quadrupole nature of this γ ray, so a spin-parity 7^+ is assigned to the 1463 keV state. This state at 1463 keV is fed by a strong 1189 keV γ-ray transition depopulating the state at 2652 keV. Previous observations predicted $E2$ nature for the 1189 keV transition, so the state at 2652 keV is assigned with a 9^+ spin-parity value. The state at 3042 keV is depopulated by 390, 531, 1268, and 1579 keV γ rays to states at 2652 (9^+), 2511, 1774, and 1463 keV (7^+), respectively. Measured R_{DCO} and $\Delta_{\rm asym}$ of the 1048 keV γ ray suggest 8^+ spin-parity for the state at 2511 keV, so measured values of those for 531 and 1579 keV transitions suggest a spin-parity value of 9^+ for the state at 3042 keV. As a result, the 390 keV ($9^+ \rightarrow 9^+$) transition could be assumed to be dipole in nature, though it has $R_{DCO} \approx 1.0$. This is possible, as the $\Delta I = 0$ transition will have the same angular correlation as that of a quadrupole one.

A negative polarization asymmetry value has been obtained for the 390 keV γ ray that decays from the 3042 keV level. Combining the measured values of polarization asymmetry and the corresponding DCO ratio, the $\Delta I = 0$, 390 keV transition can be characterized as a magnetic dipole type with the probable presence of a very small admixture of $E2$ component. Hence, the assignment of $M1(+E2)$ multipolarity has been made for the 390 keV transition. The measured R_{DCO} and $\Delta_{\rm asym}$ values of 1268 and 262 keV γ rays suggest 7^+ and 6^+ spin-parities for 1774 and 1512 keV states, respectively.

We would also like to mention here that the peak height of 1268 keV transition as can be seen from Figs. 5(c)–5(e) is not in accordance with that of the 1579 keV γ ray as far as the measured intensities of the two transitions are concerned (see Table I). Both the transitions decay from 3042 keV level and the measured intensities suggest that the height of the 1268 keV peak should be more than that of the 1579 keV peak in the gated spectra of Figs. 5(c)–5(e) obtained with the gating transitions that feed the 3042 keV level. It is worthwhile mentioning that the quoted intensities of Table I for the 1268 and 1579 keV branches have been obtained from the gated spectrum of the 253 keV γ-ray lying below the 3042 keV level. The analysis of the gated spectrum provides clear indication of a larger peak area of the 1268 keV transition in comparison to that of the 1579 keV transition. The anomalies in the peak count for 1268 and 1579 keV transitions between the top gated and bottom gated coincidence spectra may possibly reflect a missing

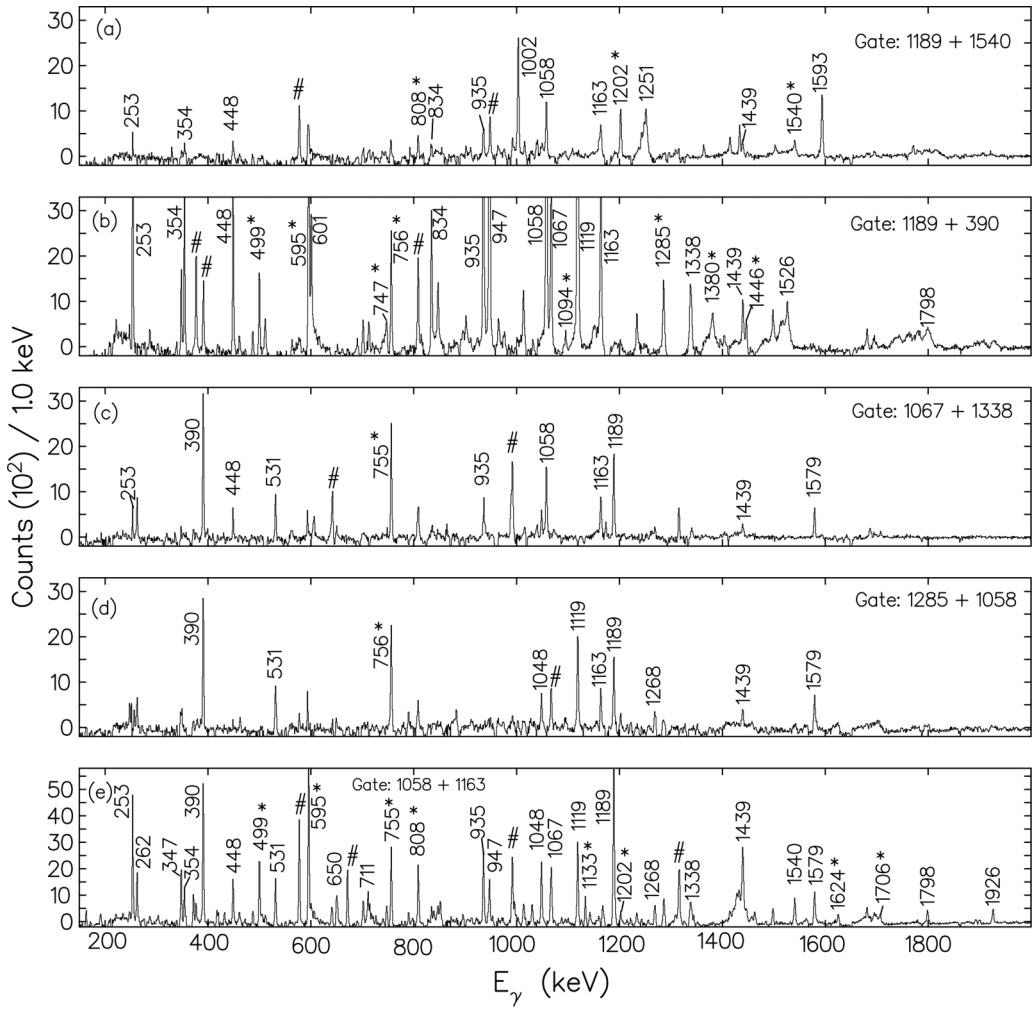

FIG. 5. Background subtracted γ-γ coincidence spectra for ^{66}Ga in the sum gates of (a) 1189 ($9^+ \rightarrow 7^+$) and 1540 keV ($10^- \rightarrow 9^+$), (b) 1189 ($9^+ \rightarrow 7^+$) and 390 keV ($9^+ \rightarrow 9^+$), (c) 1067 ($10^+ \rightarrow 9^+$) and 1338 keV ($12^{(+)} \rightarrow 10^+$), (d) 1285 ($13^+ \rightarrow 12^+$) and 1058 keV ($15^+ \rightarrow 13^+$), and (e) 1058 ($15^+ \rightarrow 13^+$) and 1163 keV ($17^+ \rightarrow 15^+$) γ rays. New transitions are marked by asterisks ($*$). The inset of (e) contains the portion of 1058 + 1163 keV gated spectrum (from 1600 to 1800 keV in energy in the x axis, and 0 to 800 in counts in the y axis), which is expanded to show the presence of newly observed (weak) 1624 and 1706 keV γ rays. A few strong peaks are marked with "#" symbols indicating contaminant γ rays or ones which could not be placed in the level scheme.

1268 keV doublet transition. This missing weak doublet transition is probably in coincidence with the 253 keV γ ray and not in coincidence with either the cascade transitions of 1285, 1058, and 1163 keV or the cascade transitions of 1067 and 1338 keV. However, the doublet nature of the 1268 keV transition could not be confirmed from the present analysis.

Spin-parities of both 1141 and 721 keV states are assigned to be 4^+ and 3^+, depending upon the measured R_{DCO} of 372 and 420 keV γ rays. Here, the measured R_{DCO} and Δ_{asym} of 372 keV suggest $E2$ nature for this transition. No information regarding the spin-parity of the 1141 keV state was given by previous work. Also, the state at 721 keV was assigned with a tentative spin 3 but definite positive parity [i.e., $(3)^+$] in Ref. [10], but, as mentioned, we assign definite spin-parity to this state, from the derived multipolarity nature of 372 ($E2$) and 420 keV ($M1/E2$) transitions. The 44 and 234 keV states are reported to be 1^+ and 2^+ by previous observations [10,16,17,20,23]. Due to weak intensities of 190 and 487 keV γ rays, measurement of R_{DCO} and Δ_{asym} of these two transitions, depopulating the 234 and 721 keV states respectively, was not possible.

Measured R_{DCO} and Δ_{asym} of 1363 keV transition predicts its dipole nature to be of electric type, therefore a 10^- spin-parity is assigned to the state at 4015 keV. Following the measured R_{DCO} and Δ_{asym} of the 1540 keV γ ray and a previous assignment [10], a 10^- spin-parity value is confirmed for the state at 4192 keV.

Here, a notable fact is that the 935 keV γ-ray transition depopulating the 1350 keV (5^+) state is visible in the spectrum gated by 1189 and 1540 keV γ rays [panel (a), Fig. 5], while 601 keV γ- ray depopulating the 1463 keV (7^+) state is not. However, this 601 keV transition is also in coincidence with the 1189 and 1540 keV γ rays and has a strong peak area with sufficient statistics. This 7^+ state is an isomeric state with a half-life of 57 ns. If the coincidence time window used during the experiment was small compared to the 57 ns half-life then

TABLE I. Values of the level energy (E_i) in keV, γ-ray energy (E_γ) in keV, initial spin-parity (I_i^π) $\rightarrow$ final (I_f^π), intensity (I_γ), DCO ratio (R_{DCO}), polarization asymmetry (Δ_{asym}) and multipolarity assignment of the γ-ray transitions, as obtained in ^{66}Ga.

Level energy[a] E_i (keV)	Gamma-ray energy E_γ (keV)	Initial$\rightarrow$final spin-parity $I_i^\pi \rightarrow I_f^\pi$	Relative intensity I_γ	DCO ratio R_{DCO}	Polarization asymmetry Δ_{asym}	Assignment
161.5(4)	95.9(3)	$3^+ \rightarrow (2)^+$	100	0.62(7)[b]		$(M1+E2)$
234.02(23)	190.21(23)	$2^+ \rightarrow 1^+$	0.21(7)			
414.4(4)	252.93(24)	$4^+ \rightarrow 3^+$	87.76(95)	0.42(4)[b]	−0.09(1)	$M1+E2$
	348.61(23)[h]	$4^+ \rightarrow (2)^+$				
515.5(4)	353.83(18)	$4^+ \rightarrow 3^+$	2.50(27)	0.43(7)[b]	−0.09(1)	$M1+E2$
	450.36(12)	$4^+ \rightarrow (2)^+$	3.04(29)			
720.8(3)	486.74(20)[h]	$3^+ \rightarrow 2^+$				
	655.37(18)	$3^+ \rightarrow (2)^+$	0.20(4)			
862.6(4)	347.39(28)	$5^+ \rightarrow 4^+$	0.53(19)	0.70(25)[b]		$M1+E2$
	448.22(19)	$5^+ \rightarrow 4^+$	29.82(53)	0.41(5)[b]	−0.11(2)	$M1+E2$
	701.1(3)	$5^+ \rightarrow 3^+$	0.68(12)			
1140.8(4)	419.7(4)	$4^+ \rightarrow 3^+$	0.21(7)	0.60(28)[c]		$M1+E2$
	726.40(19)	$4^+ \rightarrow 4^+$	2.75(22)			
1349.5(4)	208.62(10)	$5^+ \rightarrow 4^+$	0.71(13)			
	486.94(15)	$5^+ \rightarrow 5^+$	3.88(24)	0.96(29)[b]	−0.03(2)	$(M1+E2)$
	834.13(13)	$5^+ \rightarrow 4^+$	3.29(38)	0.52(7)[b]	$\approx$0	$(M1+E2)$
	934.89(16)	$5^+ \rightarrow 4^+$	40.96(68)	0.45(5)[b]	−0.08(3)	$M1$
1463.3(4)	113.70(24)	$7^+ \rightarrow 5^+$	12.33(34)	0.98(7)[b]		Q
	600.67(10)	$7^+ \rightarrow 5^+$	18.21(94)	0.85(8)[b]	+0.05(1)	$E2$
1512.2(4)	162.5(3)	$6^+ \rightarrow 5^+$	1.93(27)	0.54(13)[c]		(D)
	371.69(30)	$6^+ \rightarrow 4^+$	1.17(18)	0.86(32)[c]	+0.10(3)	$E2$
	649.52(13)	$6^+ \rightarrow 5^+$	5.02(37)	0.77(27)[c]	$\approx$0	$M1+E2$
1773.9(4)	261.68(16)	$7^+ \rightarrow 6^+$	3.45(22)	0.65(7)[c]	−0.34(16)	$M1+E2$
2511.3(4)	1047.90(11)	$8^+ \rightarrow 7^+$	4.41(32)	1.28(24)[d]	−0.03(2)	$M1+E2$
2651.9(4)	1188.64(12)	$9^+ \rightarrow 7^+$	11.83(33)	1.06(10)[d]	+0.08(3)	$E2$
2790.7(5)	1327.36(22)		0.35(10)			
3042.1(4)	390.24(12)	$9^+ \rightarrow 9^+$	6.06(26)	1.08(8)[b]	−0.10(1)	$M1(+E2)$
	530.72(17)	$9^+ \rightarrow 8^+$	2.25(21)	0.53(7)[d]	−0.03(1)	$M1$
	1268.20(16)	$9^+ \rightarrow 7^+$	4.88(25)	0.92(14)[d]	+0.22(7)	$E2$
	1578.87(15)	$9^+ \rightarrow 7^+$	3.26(21)	1.12(13)[d]	+0.03(2)	$E2$
3181.7(5)	670.40(17)		0.90(14)			
3249.1(7)	1899.6(5)[h]					
3362.8(5)	710.92(24)	$(9^+) \rightarrow 9^+$	0.72(16)	1.11(26)[b]	−0.06(5)	$(M1+E2)$
3503.0(6)	851.1(4)	$(9^+) \rightarrow 9^+$	0.31(11)	1.12(44)[b]		$(M1+E2)$
4015.2(4)	1363.41(10)	$10^- \rightarrow 9^+$	0.40(8)	0.54(8)[b]	+0.03(2)	$E1$
	1503.79(18)	$10^- \rightarrow 8^+$	0.23(8)	1.07(60)[f]		(Q)
4073.8(4)	1562.48(13)		0.60(8)			
4109.0(4)	1066.81(14)	$10^+ \rightarrow 9^+$	1.16(14)	0.37(7)[b]	+0.09(7)	$M1+E2$
4160.7(4)	1118.70(16)	$11^+ \rightarrow 9^+$	10.66(29)	1.05(10)[b]	+0.11(2)	$E2$
4192.0(4)	1540.08(14)	$10^- \rightarrow 9^+$	0.53(8)	0.69(9)[e]	+0.10(2)	$E1^g$
4495.3(5)	1132.5(3)	$(11^+) \rightarrow (9^+)$	0.66(7)	1.07(36)[b]		(Q)
4577.5(5)	1925.58(17)	$10^- \rightarrow 9^+$	0.49(8)	0.56(13)[b]		$E1^g$
4916.2(5)	755.58(12)	$12^+ \rightarrow 11^+$	0.95(10)			
5000.0(5)	808.08(24)	$12^{(-)} \rightarrow 10^-$	0.87(18)	0.83(14)[b]		Q
5107.5(5)	946.75(12)	$13^+ \rightarrow 11^+$	5.90(22)	0.92(8)[b]	+0.11(2)	$E2$
5446.9(5)	1337.75(18)	$(12^+) \rightarrow 10^+$	0.88(12)	0.85(27)[b]		(Q)
5686.5(5)	1525.80(22)[h]	$12^- \rightarrow 11^+$				
5703.0(5)	595.45(13)	$(12^+) \rightarrow 13^+$	3.56(50)	0.60(11)[d]	−0.41(9)	$M1+E2$
5785.3(4)	1593.28(15)	$12^- \rightarrow 10^-$	0.32(9)	0.93(30)[b]		$E2^g$
	1770.04(12)	$12^- \rightarrow 10^-$	0.87(25)	1.29(68)[f]		$E2$
5844.0(5)	1770.22(25)[h]					
6201.8(4)	498.77(19)	$13^+ \rightarrow (12^+)$	2.17(29)	0.59(7)[d]	−0.06(4)	$M1+E2$
	754.81(18)	$13^+ \rightarrow 12^{(+)}$	0.57(7)			
	1094.4(4)[h]	$13^+ \rightarrow 13^+$				
	1201.85(17)	$13^+ \rightarrow 12^{(-)}$	0.59(10)	0.57(15)[b]		$(D+Q)$

TABLE I. *(Continued).*

Level energy[a] E_i (keV)	Gamma-ray energy E_γ (keV)	Initial→final spin-parity $I_i^\pi \rightarrow I_f^\pi$	Relative intensity I_γ	DCO ratio R_{DCO}	Polarization asymmetry Δ_{asym}	Assignment
	1285.69(17)	$13^+ \rightarrow 12^+$	1.10(3)	0.57(16)[b]	−0.11(5)	$M1+E2$
	1624.34(23)	$13^+ \rightarrow 10^-$	0.55(10)			
	1706.5(3)	$13^+ \rightarrow (11^+)$	0.20(7)			
6449.9(5)	746.87(22)[h]					
6487.7(5)	1380.23(23)[h]					
6787.7(5)	1002.41(16)	$14^- \rightarrow 12^-$	1.89(22)	1.16(19)[b]	+0.10(8)	$E2$
6884.9(5)	1777.39(23)[h]					
7132(3)	1445.8(26)		0.35(10)			
7181.5(11)	2074[h,i]	$14^{(-)} \rightarrow 13^+$				
7186.5(11)	2079[h,i]					
7259.7(5)	1057.87(12)	$15^+ \rightarrow 13^+$	5.05(30)	1.00(10)[b]	+0.04(1)	$E2$
8038.4(5)	1250.67(19)	$16^- \rightarrow 14^-$	0.57(14)	0.82(17)[f]		Q
8422.6(6)	1162.9(4)	$17^+ \rightarrow 15^+$	4.05(20)	0.88(9)[b]	+0.07(2)	$E2$
9578.4(11)	1540[h,i]					
9861.6(7)	1438.95(20)	$19^{(+)} \rightarrow 17^+$	0.72(11)	1.03(10)[e]		Q
11264.9(12)	1686.44(11)		0.34(9)			
11659.3(7)	1797.7(3)	$21^{(+)} \rightarrow 19^{(+)}$	0.67(11)	0.90(26)[e]		Q

[a]Level energies are obtained from least-squares fit to the γ energies using the GTOL code [22].
[b]Gate on $E2$, 1189 keV.
[c]Gate on $E2$, 1268 keV.
[d]Gate on $E2$, 947 keV.
[e]Gate on $E2$, 1058 keV.
[f]Gate on $E2$, 1002 keV.
[g]Corroborated also with Ref. [10].
[h]Intensity measurement was not possible due to low statistics.
[i]γ-energy error of 1 keV was assumed to get least-squares fit level energy.

some of that coincidence intensity would be lost, but it was ≈250 ns. So, coincidence time window is probably not the reason behind this. The reason for the disappearance of the 601 keV transition in the sum gate of 1189 and 1540 keV γ rays is not confirmed in this work.

A positive parity band was observed by the authors of Ref. [10], and was reported to be built on the 11^+ state, consisting of 947, 1058, 1163, 1439, and 1799 keV γ rays depopulating, respectively, states at 5108 (13^+), 6167 (15^+), 7330(17^+), 8769 ($19^{(+)}$), and 10568 keV ($21^{(+)}$). Now, it is evident in the gated spectra (Fig. 5) that 1058, 1163, and 1439 keV γ rays are in coincidence with 1338 and 1067 keV transitions. So, a new linking transition of 755 keV (6202 → 5447 keV) has been placed connecting former transitions with 1338 and 1067 keV transitions depopulating the states at 5447 and 4109 keV, respectively. As a result, the previously reported positive parity yrast band has been modified and the energy values of the states depopulated by 1058, 1163, 1439, and 1798 keV γ rays have been changed to 7260 (15^+), 8423 (17^+), 9862 ($19^{(+)}$), and 11 659 keV ($21^{(+)}$) respectively. The state at 5108 keV decays to the 9^+ (3042 keV) state via two strong 947 and 1119 keV γ rays in cascade. The measured values of R_{DCO} and Δ_{asym} of the former two transitions suggest 13^+ and 11^+ spin-parity values for states at 5108 and 4161 keV, respectively.

The state at 6202 keV, which is newly observed in this work, decays mainly by fragmented γ rays of 755, 499, 1094, 1285, 1202, 1624, and 1706 keV energy to the states at 5447, 5703, 5108, 4916, 5000, 4578, and 4495 keV, respectively. The fragmented decay pattern of the former state suggests that the wave function corresponding to this state is of complex nature. This state decays to that at 5108 keV (13^+) via the cascade of two newly observed 499 and 595 keV γ rays as well as by the direct 1094 keV transition. Measured values of the DCO ratio of newly observed 1202 and 808 keV transitions suggest a spin value of 13 for the state at 6202 keV, while the measured values of DCO ratio and polarization asymmetry of 499 and 595 keV transitions confirm positive parity for this state. The state at 5703 keV is assigned with a tentative spin-parity 12^+, based on the assigned spin-parities of the states at 6202 and 5108 keV, and further it is confirmed by the measured DCO ratio and polarization asymmetry values of 499 and 595 keV transitions.

Measured values of DCO ratio and polarization asymmetry of 595 keV γ ray do suggest a 14^+ spin-parity value for the state at 5703 keV. But in that case measured values of DCO ratio and polarization asymmetry of 499 keV transition would suggest 15^+ spin-parity for the 6202 keV state. As a result, many of the γ-ray transitions depopulating this 6202 keV state would have ambiguous multipolarities; for example, the 755 keV γ ray would be $M3$ in nature and the 1624 keV one would be $E5$ in nature. So, a tentative 12^+ spin-parity is assigned to the 5703 keV state.

The state at 6202 keV also decays to that at 4161 keV via the cascade of 1285 and 756 keV γ rays, and the measured values of DCO ratio and polarization asymmetry of the

1285 keV γ ray predict a spin-parity of 12^+ for the state at 4916 keV. Interestingly, the state at 6202 keV decays to that at 4578 keV via a 1624 keV $E3$ type γ ray. The $E3$ type transition is observed for the first time in this nucleus in the present work, but, due to very low intensity of this γ ray, measurements of R_{DCO} and Δ_{asym} were not possible.

Here, an important fact is that the 499 and 595 keV transitions should have similar peak areas when gated from above, but the 595 keV γ ray appears with a nearly double peak area compared to the 499 keV γ-ray as is evident from gated spectrum (e) of Fig. 5. This could be due to the presence of a 595 keV doublet or could reflect missing transitions, which is not confirmed by the present observation.

The spin-parities of the states at 8423 and 7260 keV are estimated to be 17^+ and 15^+, respectively, from the observed stretched electric quadrupole nature of both the depopulating 1163 and 1058 keV γ rays. The measured R_{DCO} value of the 1439 keV γ ray suggests stretched quadrupole nature of this transition but, as polarization measurement was not possible due to low intensity of this transition, a tentative positive parity is assigned to the state at 9862 keV. The state at 11 659 keV is assigned $21^{(+)}$ spin-parity value, based on the measured R_{DCO} value of the 1798 keV transition.

Placement of the state at 5447 keV was tentative in previous work [10], but its presence is confirmed in the present experiment, as we could detect the depopulating 1338 keV γ ray in strong coincidence with the 1067 keV transition and other strong and weak transitions in cascade, as shown in the gated spectra (Fig. 5).

The 5446 keV level decays through a single branch of the 1338 keV transition. The level is found to be populated very weakly in the present experiment. Hence, the extracted DCO value of the 1338 keV transition is associated with a large uncertainty and a tentative (12^+) assignment has been made for the 5446 keV level.

The state at 3363 keV is assigned with a tentative spin-parity of (9^+) based on the measured values of R_{DCO} and Δ_{asym} of the 711 keV transition decaying from the 3363 keV level. Previously, it was assigned as 10^+ [10]. The measured values of R_{DCO} and Δ_{asym} for the 711 keV transition suggest that the state at 3363 keV could perhaps be assigned with a spin-parity value of 11^-, but in that case the 711 keV γ ray would be of $M2$ multipolarity which is supposed to be less probable. Here, the measured uncertainty in R_{DCO} also suggests that the 711 keV transition may have considerable mixing, so a tentative $(M1 + E2)$ multipolarity is assigned to this γ ray and the state at 3363 keV is assigned tentatively with (9^+) spin-parity. Following the same assumption, the state at 3503 keV is also assigned tentatively with 9^+ spin-parity, though it is depopulated by the 851 keV γ ray which has $R_{DCO} \approx 1.0$. The state at 3363 keV is connected to that at 6202 keV via two newly observed γ rays in cascade, i.e., 1133 and 1706 keV. The new state at 4495 keV is assigned with a tentative spin-parity 11^+, on the basis of the measured value of DCO ratio of the 1133 keV γ ray transition. The negative parity state at 8038 keV decays to that at 4192 keV by 1251, 1002, and 1593 keV γ rays in cascade. Measured R_{DCO} and Δ_{asym} predict stretched quadrupole nature of electric type for the 1002 keV γ ray and the measured R_{DCO} for 1251 and 1593 keV transitions suggest quadrupole nature. The negative-parity band has been extended up to an excitation energy $\approx$11 MeV by placing two new transitions, viz., of 1540 and 1686 keV, in cascade above the state at 8038 keV.

The 9^+ state of ^{66}Ga at 2652 keV has a single-particle origin from contributions of both the $1g_{9/2}$ proton and $1g_{9/2}$ neutron. So, the coupling of the 9^+ state with the 2^+, 3^+, 4^+, 6^+, and 8^+ states of ^{64}Zn, which has one proton and one neutron less than ^{66}Ga, can produce, respectively, 11^+, 12^+, 13^+, 15^+, and 17^+ states of ^{66}Ga. In order to search for the possibility of such coupling, we have compared (Fig. 6) the observed energy states with 11^+, 12^+, 13^+, 15^+, and 17^+ spin-parity values of ^{66}Ga with those originating from coupling of 9^+ state (at 2652 keV) of ^{66}Ga with 2^+, 3^+, 4^+, 6^+, and 8^+ states of ^{64}Zn [7,22]. In Fig. 6, a similar comparison is made in ^{68}Ga, for standardization purpose. In ^{68}Ga, the energies of 9^+, 11^+, 13^+, 15^+, and 17^+ states are taken from Ref. [12] and the National Nuclear Data Center (NNDC) [34]. In the case of ^{68}Ga, coupled states are coming from the coupling of the 9^+ state of ^{68}Ga at 2894 keV with 2_1^+, 2_2^+, 4_1^+, 6_1^+, and 8_1^+ states of ^{66}Zn [15]. As is evident from Fig. 6, the observed states are in close proximity in energy with the coupled states in the case of ^{68}Ga, compared to ^{66}Ga. Variation in energy with spin for the observed states follows the same pattern as that of the coupled states, in the case of ^{68}Ga, but does not follow the pattern in the case of ^{66}Ga. The energy states at 12^+ and 17^+ are lower in energy with respect to $9^+ \otimes 3_1^+$ and $9^+ \otimes 8_1^+$ coupled states, respectively, whereas the energy values of yrast 11^+, 13^+, and 15^+ states are higher than those of $9^+ \otimes 2_1^+$, $9^+ \otimes 4_1^+$, and $9^+ \otimes 6_1^+$ coupled states, respectively. All the observed states are lower in energy values compared to the coupled states, in the case of ^{68}Ga. The reason behind this behavior could be due to the complex interaction nature between the core and particles in the case of ^{66}Ga compared to ^{68}Ga. As far as the residual interactions between the core and particles are concerned, we may infer from this observation that ^{66}Zn is behaving more as a pure core than ^{64}Zn. This nature of the vibrating core, in the case of ^{68}Ga, gives rise to a platform for more simple kinds of excitations at intermediate and high spins, compared to ^{66}Ga. Therefore, a complex nature of excitations in ^{66}Ga draws special attention to explore the fundamental single-particle configurations related to its structure.

IV. SHELL MODEL CALCULATIONS

In order to understand the observed nuclear structure in ^{66}Ga, shell model calculations have been performed in the present work using two different interactions, viz., jun45pn [35] and jj44bpn [36]. The shell model code NuShellX@MSU [37] was used for this purpose. With the ^{56}Ni core, the valence space for the calculation consists of $2p_{3/2}$, $1f_{5/2}$, $2p_{1/2}$, and $1g_{9/2}$ proton and neutron orbitals. The effective Hamiltonian jun45pn [35] has been obtained from a realistic interaction based on the Bonn-C potential, with a total of 133 two-body matrix elements and four single-particle energies modified empirically so as to fit 400 experimental energy values of 69 nuclei with mass numbers $A = 63$–96. In the derivation of this effective Hamiltonian, experimental

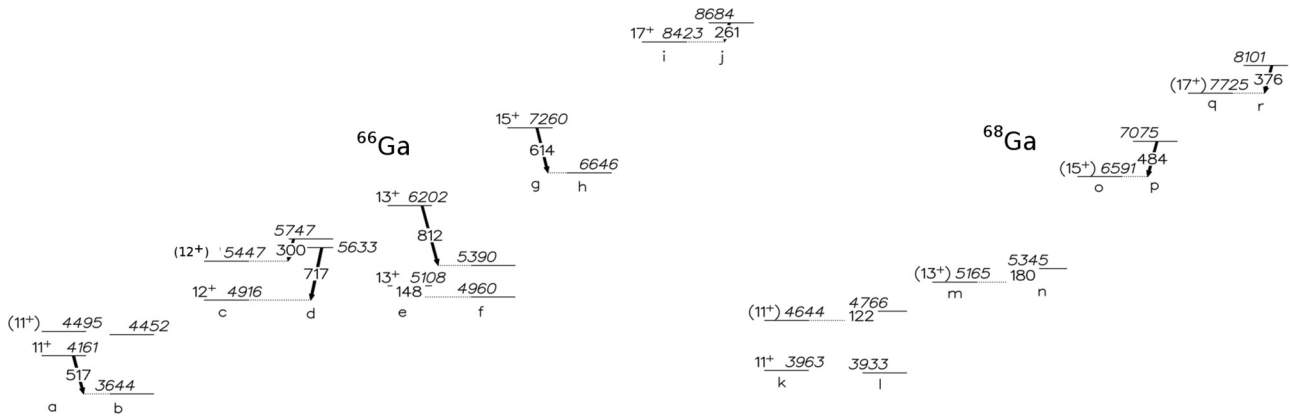

FIG. 6. A comparison of observed states with coupled states in ^{66,68}Ga. Panel a: Observed energy states of 11^+_1 and 11^+_2 in ^{66}Ga obtained from the present experiment. Panel b: Calculated sum energy of the 9^+_1 state of ^{66}Ga (2652 keV, observed in the present experiment) plus 2^+_1, 2^+_2 of ^{64}Zn [7,22], producing coupled states 11^+_1 and 11^+_2 of ^{66}Ga. Similarly, panels (c and d), (e and f), (g and h), and (i and j) for different mentioned states in ^{66}Ga. Here, the observed states compared are 11^+, 12^+, 13^+, 15^+, and 17^+ of ^{66}Ga. Panel k: Observed energy states of 11^+_1 and 11^+_2 in ^{68}Ga [12]. Panel l: Calculated sum energy of 9^+ state of ^{68}Ga [12] plus 2^+_1, 2^+_2 of ^{66}Zn [15], producing coupled states 11^+_1 and 11^+_2 of ^{68}Ga. Similarly, panels (m and n), (o and p), and (q and r) for different mentioned states in ^{68}Ga. Here, the observed states compared are 11^+, 13^+, 15^+, and 17^+ of ^{68}Ga. Each arrow represents the energy difference between the observed and coupled states (true for all pairs > 100 keV apart, for visualization purpose). See text for details.

data are not taken from $N = Z$ nuclei, specifically the Ni and Cu isotopes, because the model space may not be sufficient to describe the collectivity expected in these nuclei. The single-particle energies for this Hamiltonian are −9.8280, −8.7087, −7.8388, and −6.261 MeV, respectively for the $2p_{3/2}$, $1f_{5/2}$, $2p_{1/2}$, and $1g_{9/2}$ orbitals. The effective Hamiltonian jj44bpn, due to Brown and Lesitskiy [36], is a realistic interaction based on the Bonn-C potential, which has been obtained by fitting binding energies and excitation energies in the Ni, Cu, and Zn isotopes and nuclei close to $N = 50$. The single-particle energies are taken to be −9.6566, −9.2859, −8.2695, and −5.8944 MeV for the $2p_{3/2}$, $1f_{5/2}$, $2p_{1/2}$, and $1g_{9/2}$ orbitals, respectively. Previous calculations for ^{63}Zn [5], ^{63}Cu [29], and ^{60,62,64,66}Zn [38] with similar interaction and model space have produced very good agreements.

Observed levels in the present experiment, which are assigned with definite or tentative spin-parities, are compared with shell model calculations in Fig. 7. Those observed levels which are not assigned with spin-parities are not compared with calculated levels. The dominant particle configurations, constituting the wave functions of the levels, are represented in Tables II and III.

We have calculated occupation probabilities of protons and neutrons for two different interactions, and the results of these calculations are presented in Figs. 8–13. The wave function of a shell model state is the superposition of different orbitals included in the valence space, and occupation probability corresponding to an orbital indicates the fraction of the total number of valence nucleons (either protons or neutrons) occupying that particular orbital. So, an occupation probability gives the strength of individual contributions of different orbitals ($2p_{3/2}$, $1f_{5/2}$, $2p_{1/2}$, and $1g_{9/2}$ orbitals in the present calculation) of both the protons and neutrons in the total wave function.

Shell model calculations with jj44bpn interaction predict the first 1^+ state at just 27 keV higher in energy value with respect to the observed value, but it is 142 keV higher in energy value as obtained by using the jun45pn interaction. So, the jj44bpn interaction produces the energy of the 1^+ state better than the jun45pn interaction. The energy of the first excited 3^+ state is better predicted by the jun45pn interaction than by the jj44bpn interaction but both fail to produce the energy value of the second excited 3^+ state, giving a result ≈350 keV lower in energy than the experimental value. The configuration of the first excited 3^+ state is predicted to be $[(\pi(p_{3/2})^3]_{j_p=3/2} \otimes [\nu(f_{5/2})^3(p_{3/2})^4]_{j_\nu=5/2}$ (probability ≈13%) by jun45pn (Table III). Energies of the first and the second excited 5^+ states are well predicted by the jun45pn interaction, while they are overpredicted by the jj44bpn interaction. The predicted configurations by the jun45pn interaction for these states are $[\pi(f_{5/2})^1(p_{3/2})^2]_{j_p=5/2} \otimes [\nu(f_{5/2})^3(p_{3/2})^4]_{j_\nu=5/2}$ (probability ≈15%) and $[\pi(p_{3/2})^3]_{j_p=3/2} \otimes [\nu(f_{5/2})^3(p_{3/2})^4]_{j_\nu=9/2}$ (probability ≈11%), respectively. Neither interaction could produce the energy values of the first and the second excited 7^+ states, and shell model calculated values are far above the observed values. It is evident from the occupation number plots (Figs. 8 and 9) that significant contributions are coming from the $g_{9/2}$ proton and neutron orbitals in the case of the first 7^+ state, as calculated by the jj44bpn interaction. From the configuration tables of wave functions (Tables II and III), it is clear that the configurations with the highest probability for the first excited 7^+ states are $[\pi(p_{3/2})^1(p_{1/2})^1(g_{9/2})^1]_{j_p=5/2} \otimes [\nu(f_{5/2})^2(p_{3/2})^4(g_{9/2})^1]_{j_\nu=9/2}$ (probability ≈2%) and $[\pi(f_{5/2})^1(p_{3/2})^2]_{j_p=5/2} \otimes [\nu(f_{5/2})^3(p_{3/2})^4]_{j_\nu=9/2}$ (probability ≈11%) as predicted by jj44bpn and jun45pn interactions, respectively. Both interactions predict a full alignment of angular momenta contributed by both types of nucleons, i.e., proton and neutron, in forming the 7^+_1 state. No particular configuration appears to be dominant in forming the wave function for the first 7^+ state; rather, there is large competition between different configurations.

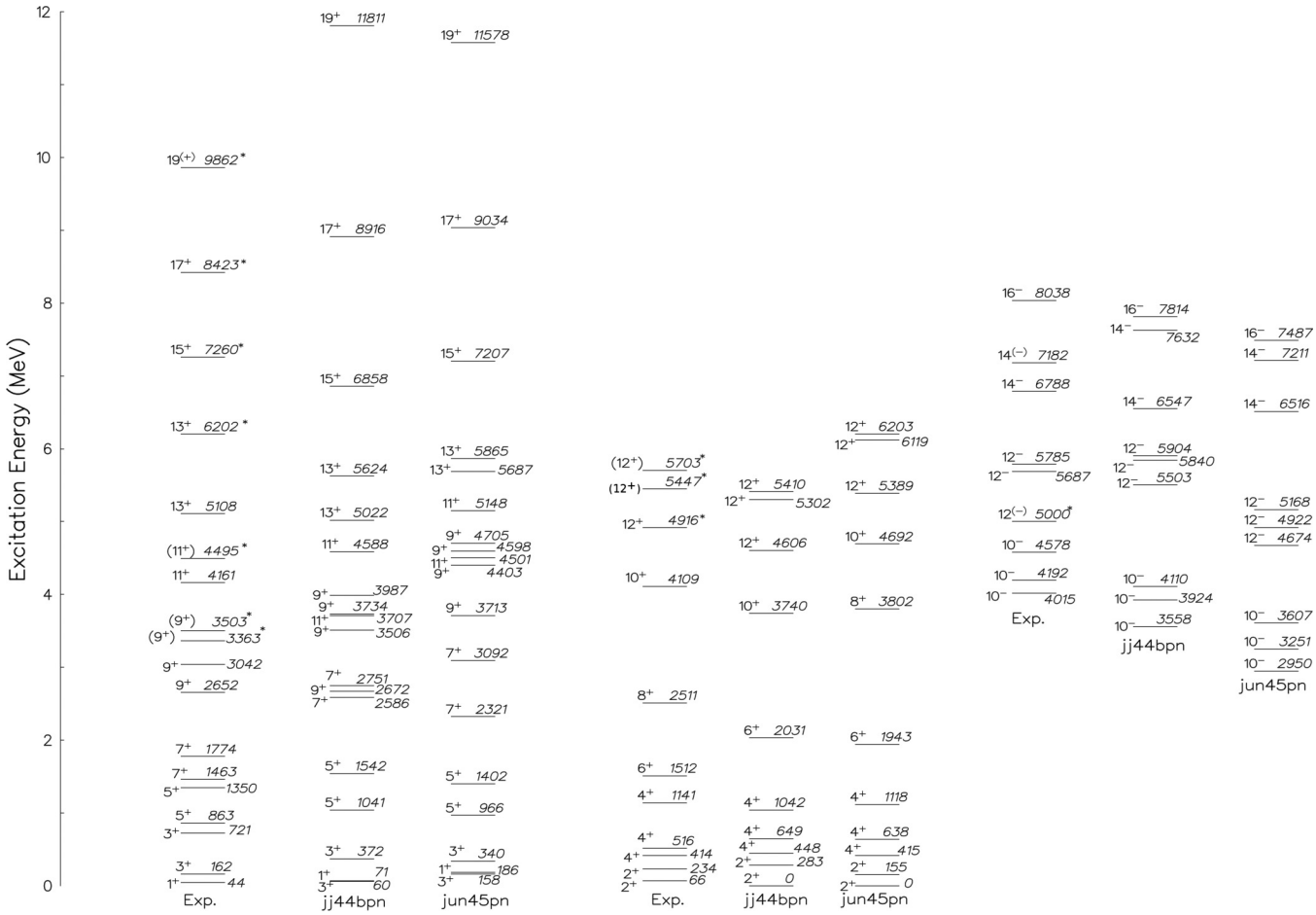

FIG. 7. Comparison of the observed levels of ^{66}Ga with shell model calculations using jj44bpn [36] and jun45pn [35] interactions. Newly observed levels in this experiment are identified with asterisks (∗). The energies in the figure are in keV.

The first 2^+ excited state is predicted by both interactions to be at 0 keV, whereas the experimental energy value is 66 keV. The second excited 2^+ state is overpredicted by the jj44bpn interaction and is underpredicted by the jun45pn interaction. Energy values of the three 4^+ states, as calculated using the jj44bpn interaction, are in moderate agreement with the observed values, whereas the jun45pn interaction predicts the proper value of 415 keV for the first excited 4^+ state, and the second and the third excited 4^+ states are also well predicted by the jun45pn interaction in comparison with jj44bpn. Configurations corresponding to these 4^+ states, as given by calculations using jun45pn

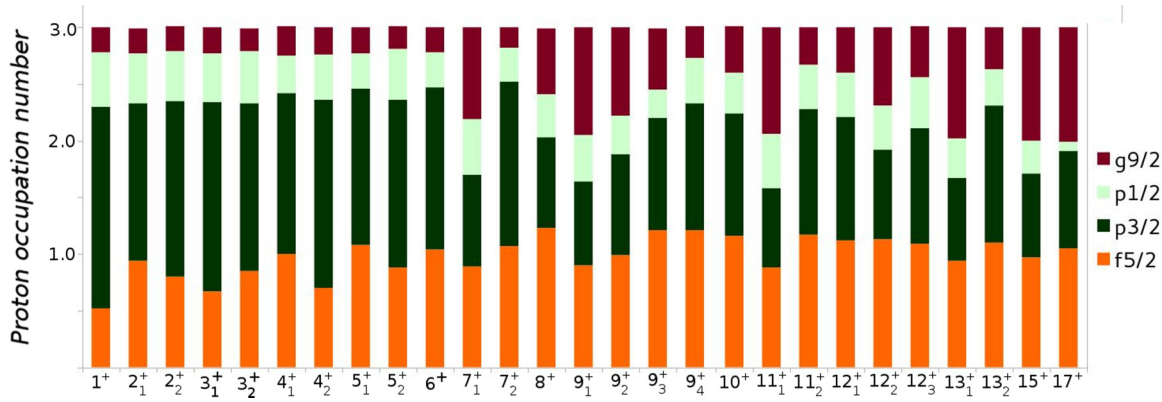

FIG. 8. Calculated occupation probabilities of the $f_{5/2}$, $p_{3/2}$, $p_{1/2}$, and $g_{9/2}$ orbitals for the positive parity states for protons in ^{66}Ga. The occupation probabilities are calculated from the shell model using the jj44bpn interaction. Please see text for details.

TABLE II. Configurations with the highest probabilities of different states in ^{66}Ga, calculated by the shell model using $f_{5/2}pg_{9/2}$ model space with jj44bpn interaction.

Spin-parity(j^π)	Configuration	Probability
	Positive parity	
1^+	$\pi(f_{5/2})^0(p_{3/2})^3(p_{1/2})^0(g_{9/2})^0 \otimes \nu(f_{5/2})^2(p_{3/2})^4(p_{1/2})^1(g_{9/2})^0$	9.03
2^+	$\pi(f_{5/2})^1(p_{3/2})^2(p_{1/2})^0(g_{9/2})^0 \otimes \nu(f_{5/2})^3(p_{3/2})^4(p_{1/2})^0(g_{9/2})^0$	3.59
3_1^+	$\pi(f_{5/2})^0(p_{3/2})^3(p_{1/2})^0(g_{9/2})^0 \otimes \nu(f_{5/2})^2(p_{3/2})^4(p_{1/2})^1(g_{9/2})^0$	3.44
3_2^+	$\pi(f_{5/2})^1(p_{3/2})^2(p_{1/2})^0(g_{9/2})^0 \otimes \nu(f_{5/2})^4(p_{3/2})^3(p_{1/2})^0(g_{9/2})^0$	4.23
4_1^+	$\pi(f_{5/2})^1(p_{3/2})^2(p_{1/2})^0(g_{9/2})^0 \otimes \nu(f_{5/2})^3(p_{3/2})^4(p_{1/2})^0(g_{9/2})^0$	4.32
4_2^+	$\pi(f_{5/2})^0(p_{3/2})^3(p_{1/2})^0(g_{9/2})^0 \otimes \nu(f_{5/2})^3(p_{3/2})^4(p_{1/2})^0(g_{9/2})^0$	5.44
4_3^+	$\pi(f_{5/2})^1(p_{3/2})^2(p_{1/2})^0(g_{9/2})^0 \otimes \nu(f_{5/2})^3(p_{3/2})^2(p_{1/2})^0(g_{9/2})^2$	1.56
5_1^+	$\pi(f_{5/2})^1(p_{3/2})^2(p_{1/2})^0(g_{9/2})^0 \otimes \nu(f_{5/2})^3(p_{3/2})^4(p_{1/2})^0(g_{9/2})^0$	9.33
5_2^+	$\pi(f_{5/2})^0(p_{3/2})^2(p_{1/2})^1(g_{9/2})^0 \otimes \nu(f_{5/2})^3(p_{3/2})^4(p_{1/2})^0(g_{9/2})^0$	4.92
6^+	$\pi(f_{5/2})^1(p_{3/2})^2(p_{1/2})^0(g_{9/2})^0 \otimes \nu(f_{5/2})^4(p_{3/2})^3(p_{1/2})^0(g_{9/2})^0$	5.17
7_1^+	$\pi(f_{5/2})^0(p_{3/2})^1(p_{1/2})^1(g_{9/2})^1 \otimes \nu(f_{5/2})^2(p_{3/2})^4(p_{1/2})^0(g_{9/2})^1$	1.93
7_2^+	$\pi(f_{5/2})^1(p_{3/2})^2(p_{1/2})^0(g_{9/2})^0 \otimes \nu(f_{5/2})^3(p_{3/2})^4(p_{1/2})^0(g_{9/2})^0$	6.87
8^+	$\pi(f_{5/2})^2(p_{3/2})^1(p_{1/2})^0(g_{9/2})^0 \otimes \nu(f_{5/2})^2(p_{3/2})^3(p_{1/2})^0(g_{9/2})^2$	2.45
9_1^+	$\pi(f_{5/2})^0(p_{3/2})^2(p_{1/2})^0(g_{9/2})^1 \otimes \nu(f_{5/2})^2(p_{3/2})^4(p_{1/2})^0(g_{9/2})^1$	4.13
9_2^+	$\pi(f_{5/2})^0(p_{3/2})^2(p_{1/2})^0(g_{9/2})^1 \otimes \nu(f_{5/2})^2(p_{3/2})^3(p_{1/2})^1(g_{9/2})^1$	4.24
9_3^+	$\pi(f_{5/2})^1(p_{3/2})^2(p_{1/2})^0(g_{9/2})^0 \otimes \nu(f_{5/2})^2(p_{3/2})^3(p_{1/2})^0(g_{9/2})^2$	5.63
9_4^+	$\pi(f_{5/2})^1(p_{3/2})^2(p_{1/2})^0(g_{9/2})^0 \otimes \nu(f_{5/2})^2(p_{3/2})^2(p_{1/2})^1(g_{9/2})^2$	2.78
10^+	$\pi(f_{5/2})^1(p_{3/2})^2(p_{1/2})^0(g_{9/2})^0 \otimes \nu(f_{5/2})^3(p_{3/2})^2(p_{1/2})^0(g_{9/2})^2$	4.10
11_1^+	$\pi(f_{5/2})^2(p_{3/2})^0(p_{1/2})^0(g_{9/2})^1 \otimes \nu(f_{5/2})^4(p_{3/2})^2(p_{1/2})^0(g_{9/2})^1$	3.15
11_2^+	$\pi(f_{5/2})^1(p_{3/2})^2(p_{1/2})^0(g_{9/2})^0 \otimes \nu(f_{5/2})^3(p_{3/2})^2(p_{1/2})^0(g_{9/2})^2$	3.73
12_1^+	$\pi(f_{5/2})^1(p_{3/2})^2(p_{1/2})^0(g_{9/2})^0 \otimes \nu(f_{5/2})^3(p_{3/2})^2(p_{1/2})^0(g_{9/2})^2$	8.48
12_2^+	$\pi(f_{5/2})^1(p_{3/2})^1(p_{1/2})^0(g_{9/2})^1 \otimes \nu(f_{5/2})^2(p_{3/2})^4(p_{1/2})^0(g_{9/2})^1$	4.88
12_3^+	$\pi(f_{5/2})^1(p_{3/2})^1(p_{1/2})^0(g_{9/2})^1 \otimes \nu(f_{5/2})^2(p_{3/2})^4(p_{1/2})^0(g_{9/2})^1$	2.11
13_1^+	$\pi(f_{5/2})^1(p_{3/2})^1(p_{1/2})^0(g_{9/2})^1 \otimes \nu(f_{5/2})^2(p_{3/2})^4(p_{1/2})^0(g_{9/2})^1$	5.07
13_2^+	$\pi(f_{5/2})^1(p_{3/2})^2(p_{1/2})^0(g_{9/2})^0 \otimes \nu(f_{5/2})^1(p_{3/2})^4(p_{1/2})^0(g_{9/2})^2$	6.29
15^+	$\pi(f_{5/2})^1(p_{3/2})^1(p_{1/2})^0(g_{9/2})^1 \otimes \nu(f_{5/2})^3(p_{3/2})^3(p_{1/2})^0(g_{9/2})^1$	10.58
17^+	$\pi(f_{5/2})^1(p_{3/2})^1(p_{1/2})^0(g_{9/2})^1 \otimes \nu(f_{5/2})^2(p_{3/2})^3(p_{1/2})^1(g_{9/2})^1$	16.62
	Negative parity	
10_1^-	$\pi(f_{5/2})^1(p_{3/2})^2(p_{1/2})^0(g_{9/2})^0 \otimes \nu(f_{5/2})^3(p_{3/2})^3(p_{1/2})^0(g_{9/2})^1$	2.76
10_2^-	$\pi(f_{5/2})^1(p_{3/2})^1(p_{1/2})^1(g_{9/2})^0 \otimes \nu(f_{5/2})^3(p_{3/2})^3(p_{1/2})^0(g_{9/2})^1$	3.61
10_3^-	$\pi(f_{5/2})^1(p_{3/2})^2(p_{1/2})^0(g_{9/2})^0 \otimes \nu(f_{5/2})^3(p_{3/2})^3(p_{1/2})^0(g_{9/2})^1$	8.99
12_1^-	$\pi(f_{5/2})^1(p_{3/2})^2(p_{1/2})^0(g_{9/2})^0 \otimes \nu(f_{5/2})^2(p_{3/2})^4(p_{1/2})^0(g_{9/2})^1$	5.51
12_2^-	$\pi(f_{5/2})^1(p_{3/2})^1(p_{1/2})^1(g_{9/2})^0 \otimes \nu(f_{5/2})^2(p_{3/2})^4(p_{1/2})^0(g_{9/2})^1$	6.43
14_1^-	$\pi(f_{5/2})^2(p_{3/2})^0(p_{1/2})^0(g_{9/2})^1 \otimes \nu(f_{5/2})^3(p_{3/2})^2(p_{1/2})^0(g_{9/2})^2$	11.78
14_2^-	$\pi(f_{5/2})^1(p_{3/2})^1(p_{1/2})^0(g_{9/2})^1 \otimes \nu(f_{5/2})^2(p_{3/2})^2(p_{1/2})^1(g_{9/2})^2$	12.58
16^-	$\pi(f_{5/2})^1(p_{3/2})^0(p_{1/2})^1(g_{9/2})^1 \otimes \nu(f_{5/2})^3(p_{3/2})^2(p_{1/2})^0(g_{9/2})^2$	9.19

interaction, are $[\pi(p_{3/2})^3]_{j_p=3/2} \otimes [\nu(f_{5/2})^3(p_{3/2})^4]_{j_\nu=5/2}$ (probability ≈20%), $[\pi(f_{5/2})^1(p_{3/2})^2]_{j_p=5/2} \otimes [\nu(f_{5/2})^3(p_{3/2})^4]_{j_\nu=5/2}$ (probability ≈13%) and $[\pi(p_{3/2})^3]_{j_p=3/2} \otimes [\nu(f_{5/2})^2(p_{3/2})^4(p_{1/2})^1]_{j_\nu=7/2}$ (probability ≈6%). It is evident that first excited 4^+ state originates from the maximum alignment of proton and neutron angular momenta, whereas the other two 4^+ states arise from the partial alignment. The 6^+ excited state is overpredicted in energy value by both interactions. Here, both occupation number plots (Figs. 8–11) and configurations of wave functions (Tables II and III), show that the 6^+ state arises mainly due to the occupation of protons and neutrons in $f_{5/2}$ and $p_{3/2}$ orbitals.

With ten valence particles and with large model space, many possible configurations arise for a given total angular momentum, as there are many different ways to distribute valence particles among the $f_{5/2}$, $p_{3/2}$, $p_{1/2}$, and $g_{9/2}$ orbitals which add up to the same spin value. So, a large number of configurations to compete with each other for the construction of the wave function for a particular state, and it is evident

TABLE III. Configurations with the highest probabilities of different states in ^{66}Ga, calculated by the shell model using $f_{5/2}pg_{9/2}$ model space with jun45pn interaction.

Spin-parity(j^π)	Configuration	Probability
	Positive parity	
1^+	$\pi(f_{5/2})^0(p_{3/2})^3(p_{1/2})^0(g_{9/2})^0 \otimes \nu(f_{5/2})^3(p_{3/2})^4(p_{1/2})^0(g_{9/2})^0$	12.27
2^+	$\pi(f_{5/2})^0(p_{3/2})^3(p_{1/2})^0(g_{9/2})^0 \otimes \nu(f_{5/2})^3(p_{3/2})^4(p_{1/2})^0(g_{9/2})^0$	15.02
3_1^+	$\pi(f_{5/2})^0(p_{3/2})^3(p_{1/2})^0(g_{9/2})^0 \otimes \nu(f_{5/2})^3(p_{3/2})^4(p_{1/2})^0(g_{9/2})^0$	12.59
3_2^+	$\pi(f_{5/2})^0(p_{3/2})^2(p_{1/2})^1(g_{9/2})^0 \otimes \nu(f_{5/2})^3(p_{3/2})^4(p_{1/2})^0(g_{9/2})^0$	12.91
4_1^+	$\pi(f_{5/2})^0(p_{3/2})^3(p_{1/2})^0(g_{9/2})^0 \otimes \nu(f_{5/2})^3(p_{3/2})^4(p_{1/2})^0(g_{9/2})^0$	20.43
4_2^+	$\pi(f_{5/2})^1(p_{3/2})^2(p_{1/2})^0(g_{9/2})^0 \otimes \nu(f_{5/2})^3(p_{3/2})^4(p_{1/2})^0(g_{9/2})^0$	12.53
4_3^+	$\pi(f_{5/2})^0(p_{3/2})^3(p_{1/2})^0(g_{9/2})^0 \otimes \nu(f_{5/2})^2(p_{3/2})^4(p_{1/2})^1(g_{9/2})^0$	6.32
5_1^+	$\pi(f_{5/2})^1(p_{3/2})^2(p_{1/2})^0(g_{9/2})^0 \otimes \nu(f_{5/2})^3(p_{3/2})^4(p_{1/2})^0(g_{9/2})^0$	15.20
5_2^+	$\pi(f_{5/2})^0(p_{3/2})^3(p_{1/2})^0(g_{9/2})^0 \otimes \nu(f_{5/2})^3(p_{3/2})^4(p_{1/2})^0(g_{9/2})^0$	10.86
6^+	$\pi(f_{5/2})^1(p_{3/2})^2(p_{1/2})^0(g_{9/2})^0 \otimes \nu(f_{5/2})^2(p_{3/2})^4(p_{1/2})^1(g_{9/2})^0$	9.90
7_1^+	$\pi(f_{5/2})^1(p_{3/2})^2(p_{1/2})^0(g_{9/2})^0 \otimes \nu(f_{5/2})^3(p_{3/2})^4(p_{1/2})^0(g_{9/2})^0$	11.22
7_2^+	$\pi(f_{5/2})^0(p_{3/2})^3(p_{1/2})^0(g_{9/2})^0 \otimes \nu(f_{5/2})^4(p_{3/2})^3(p_{1/2})^0(g_{9/2})^0$	20.98
8^+	$\pi(f_{5/2})^1(p_{3/2})^2(p_{1/2})^0(g_{9/2})^0 \otimes \nu(f_{5/2})^2(p_{3/2})^4(p_{1/2})^1(g_{9/2})^0$	10.52
9_1^+	$\pi(f_{5/2})^0(p_{3/2})^2(p_{1/2})^0(g_{9/2})^1 \otimes \nu(f_{5/2})^4(p_{3/2})^2(p_{1/2})^0(g_{9/2})^1$	8.06
9_2^+	$\pi(f_{5/2})^1(p_{3/2})^2(p_{1/2})^0(g_{9/2})^0 \otimes \nu(f_{5/2})^3(p_{3/2})^4(p_{1/2})^0(g_{9/2})^0$	18.88
9_3^+	$\pi(f_{5/2})^0(p_{3/2})^2(p_{1/2})^0(g_{9/2})^1 \otimes \nu(f_{5/2})^2(p_{3/2})^3(p_{1/2})^1(g_{9/2})^1$	5.38
9_4^+	$\pi(f_{5/2})^1(p_{3/2})^2(p_{1/2})^0(g_{9/2})^0 \otimes \nu(f_{5/2})^3(p_{3/2})^2(p_{1/2})^0(g_{9/2})^2$	2.35
	and	
	$\pi(f_{5/2})^1(p_{3/2})^2(p_{1/2})^0(g_{9/2})^0 \otimes \nu(f_{5/2})^2(p_{3/2})^3(p_{1/2})^0(g_{9/2})^2$	2.35
10^+	$\pi(f_{5/2})^1(p_{3/2})^2(p_{1/2})^0(g_{9/2})^0 \otimes \nu(f_{5/2})^2(p_{3/2})^3(p_{1/2})^0(g_{9/2})^2$	6.65
11_1^+	$\pi(f_{5/2})^0(p_{3/2})^2(p_{1/2})^0(g_{9/2})^1 \otimes \nu(f_{5/2})^4(p_{3/2})^2(p_{1/2})^0(g_{9/2})^1$	5.05
11_2^+	$\pi(f_{5/2})^1(p_{3/2})^2(p_{1/2})^0(g_{9/2})^0 \otimes \nu(f_{5/2})^3(p_{3/2})^2(p_{1/2})^0(g_{9/2})^2$	5.74
12_1^+	$\pi(f_{5/2})^1(p_{3/2})^2(p_{1/2})^0(g_{9/2})^0 \otimes \nu(f_{5/2})^3(p_{3/2})^2(p_{1/2})^0(g_{9/2})^2$	12.30
12_2^+	$\pi(f_{5/2})^2(p_{3/2})^1(p_{1/2})^0(g_{9/2})^0 \otimes \nu(f_{5/2})^3(p_{3/2})^2(p_{1/2})^0(g_{9/2})^2$	4.12
12_3^+	$\pi(f_{5/2})^0(p_{3/2})^2(p_{1/2})^0(g_{9/2})^1 \otimes \nu(f_{5/2})^3(p_{3/2})^3(p_{1/2})^0(g_{9/2})^1$	6.90
13_1^+	$\pi(f_{5/2})^1(p_{3/2})^1(p_{1/2})^0(g_{9/2})^1 \otimes \nu(f_{5/2})^4(p_{3/2})^2(p_{1/2})^0(g_{9/2})^1$	5.36
13_2^+	$\pi(f_{5/2})^1(p_{3/2})^2(p_{1/2})^0(g_{9/2})^0 \otimes \nu(f_{5/2})^3(p_{3/2})^2(p_{1/2})^0(g_{9/2})^2$	9.39
15^+	$\pi(f_{5/2})^1(p_{3/2})^1(p_{1/2})^0(g_{9/2})^1 \otimes \nu(f_{5/2})^4(p_{3/2})^2(p_{1/2})^0(g_{9/2})^1$	6.19
17^+	$\pi(f_{5/2})^1(p_{3/2})^1(p_{1/2})^0(g_{9/2})^1 \otimes \nu(f_{5/2})^2(p_{3/2})^4(p_{1/2})^0(g_{9/2})^1$	15.28
	Negative parity	
10_1^-	$\pi(f_{5/2})^1(p_{3/2})^2(p_{1/2})^0(g_{9/2})^0 \otimes \nu(f_{5/2})^3(p_{3/2})^3(p_{1/2})^0(g_{9/2})^1$	9.55
10_2^-	$\pi(f_{5/2})^1(p_{3/2})^2(p_{1/2})^0(g_{9/2})^0 \otimes \nu(f_{5/2})^3(p_{3/2})^3(p_{1/2})^0(g_{9/2})^1$	7.72
10_3^-	$\pi(f_{5/2})^1(p_{3/2})^2(p_{1/2})^0(g_{9/2})^0 \otimes \nu(f_{5/2})^2(p_{3/2})^3(p_{1/2})^1(g_{9/2})^1$	9.51
12_1^-	$\pi(f_{5/2})^1(p_{3/2})^2(p_{1/2})^0(g_{9/2})^0 \otimes \nu(f_{5/2})^2(p_{3/2})^3(p_{1/2})^1(g_{9/2})^1$	14.64
12_2^-	$\pi(f_{5/2})^1(p_{3/2})^2(p_{1/2})^0(g_{9/2})^0 \otimes \nu(f_{5/2})^2(p_{3/2})^4(p_{1/2})^0(g_{9/2})^1$	8.40
14_1^-	$\pi(f_{5/2})^0(p_{3/2})^2(p_{1/2})^0(g_{9/2})^1 \otimes \nu(f_{5/2})^3(p_{3/2})^2(p_{1/2})^0(g_{9/2})^2$	9.04
14_2^-	$\pi(f_{5/2})^1(p_{3/2})^2(p_{1/2})^0(g_{9/2})^0 \otimes \nu(f_{5/2})^3(p_{3/2})^3(p_{1/2})^0(g_{9/2})^1$	12.95
16^-	$\pi(f_{5/2})^1(p_{3/2})^0(p_{1/2})^1(g_{9/2})^1 \otimes \nu(f_{5/2})^3(p_{3/2})^2(p_{1/2})^0(g_{9/2})^2$	8.12

that, for almost all the lower excited states up to 9_3^+ and 6^+, as calculated respectively by jun45pn and jj44bpn interactions in ^{66}Ga, the dominant contributions come from the fp shell. It is evident from the wave function tables (Tables II and III) that, up to the 6^+ spin state, the probability of a particular dominant configuration is significantly larger when calculated using the jun45pn interaction compared to that using jj44bpn. The energy values of 3_1^+, 4_1^+, 4_2^+, 4_3^+, 5_1^+, and 5_2^+ states, as calculated using the jun45pn interaction, are in better agreement with the experimental values, whereas only that of the 2_2^+ state calculated using the jj44bpn interaction is in good agreement with the observation. So, as far as the lower excited states are concerned, the jun45pn interaction is more efficient than the jj44bpn interaction in producing the level structure.

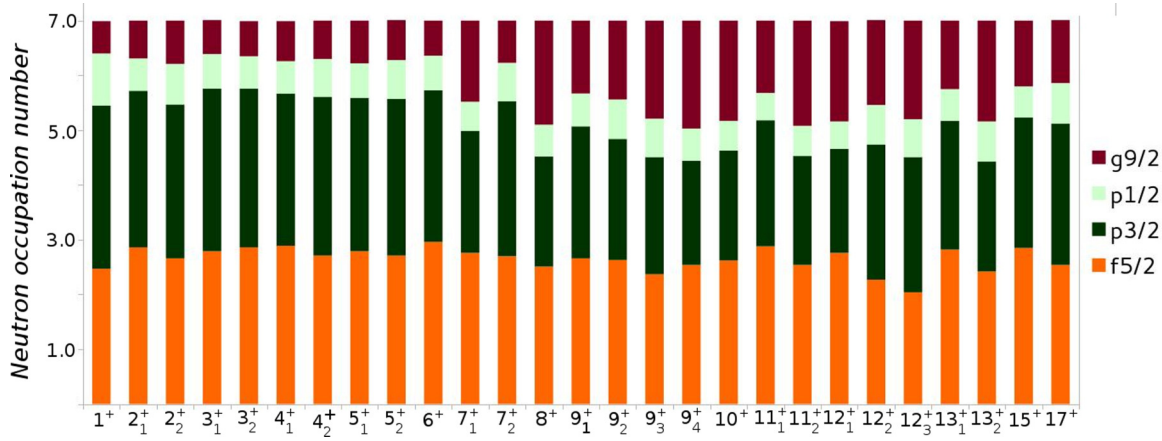

FIG. 9. Calculated occupation probabilities of the $f_{5/2}$, $p_{3/2}$, $p_{1/2}$, and $g_{9/2}$ orbitals for the positive parity states for neutrons in ^{66}Ga. The occupation probabilities are calculated from the shell model using the jj44bpn interaction. Please see text for details.

The first excited 9^+ state is well reproduced by the jj44bpn interaction but the other three 9^+ states are overpredicted by the same interaction. Here, all the 9^+ excited states are overpredicted by the jun45pn interaction. Among the different 11^+, 12^+, 13^+, and 15^+ states, the energies of the second 11^+, second 12^+, and first 13^+ states, respectively, with configurations $[\pi(f_{5/2})^1(p_{3/2})^2]_{j_p=5/2} \otimes [\nu(f_{5/2})^3(p_{3/2})^2(g_{9/2})^2]_{j_\nu=17/2}$ (probability ≈4%), $[\pi(f_{5/2})^1(p_{3/2})^1(g_{9/2})^1]_{j_p=15/2} \otimes [\nu(f_{5/2})^2(p_{3/2})^4(g_{9/2})^1]_{j_\nu=9/2}$ (probability ≈5%), and $[\pi(f_{5/2})^1(p_{3/2})^1(g_{9/2})^1]_{j_p=17/2} \otimes [\nu(f_{5/2})^2(p_{3/2})^4(g_{9/2})^1]_{j_\nu=9/2}$ (probability ≈5%) are, as predicted by the jj44bpn interaction, in good agreement with the experimental values, whereas only the energy state of 15^+ with the configuration $[\pi(f_{5/2})^1(p_{3/2})^1(g_{9/2})^1]_{j_p=17/2} \otimes [\nu(f_{5/2})^4(p_{3/2})^2(g_{9/2})^1]_{j_\nu=13/2}$ (probability ≈6%) is well reproduced by jun45pn interaction. As far as intermediate and high spin positive parity states are concerned, energy values calculated by both the interactions are in moderate agreement with the observed values but, compared to jun45pn, the jj44bpn interaction is more able to reproduce the intermediate and high spin structure within the given $f_{5/2}pg_{9/2}$ model space. In all the intermediate and high spin states in ^{66}Ga, contributions to the wave functions are mainly dominated by the $f_{5/2}$, $p_{3/2}$, and $g_{9/2}$ proton and neutron orbitals, as is obvious from the occupation probability plots and from the tables of configurations.

Higher spin states like 19^+ and above, for which the energy values as calculated by both interactions are greater than 1 MeV compared to the observed values, are not shown in configuration tables or occupation plots. So, it could be argued that a new mode of excitations is appearing at such high spin, which is different from single-particle nature. Large mixing of various orbitals at higher spins, predicted by the shell model calculations, also confirms the nature of a typical onset of collective behavior. A significant contribution, coming from $g_{9/2}$ proton and $g_{9/2}$ neutron orbitals, is very prominent, as reflected in the occupation number plots.

Three 10^- negative parity states are underpredicted in energy by both interactions, and the configurations for these states are mainly contributed from the protons in $f_{5/2}$ and $p_{3/2}$ orbitals and the neutrons in $f_{5/2}$, $p_{3/2}$, and $g_{9/2}$ orbitals. The second and the third 12^- excited states, as calculated by the jj44bpn interaction, are in good agreement, whereas the first 12^- excited state is overpredicted by the same interaction. Here, all the 12^- states are underpredicted by the jun45pn interaction. The second excited 14^- state is well predicted by the jun45pn

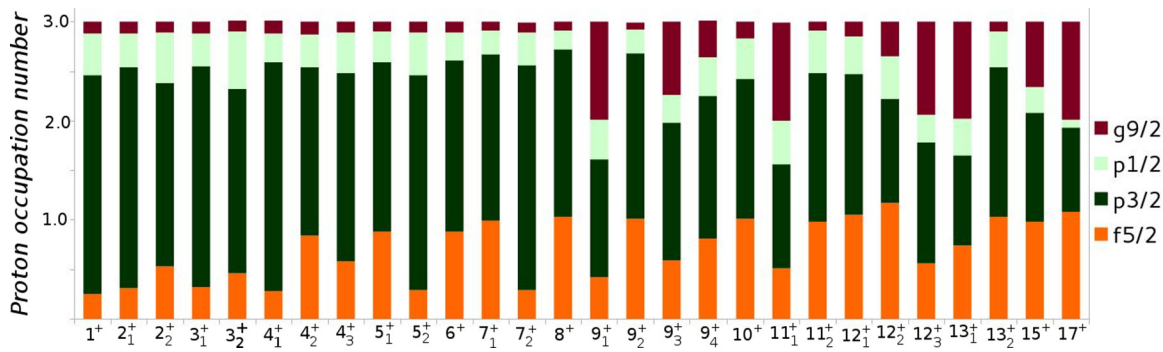

FIG. 10. Calculated occupation probabilities of the $f_{5/2}$, $p_{3/2}$, $p_{1/2}$, and $g_{9/2}$ orbitals for the positive parity states for protons in ^{66}Ga. The occupation probabilities are calculated from the shell model using the jun45pn interaction. Please see text for details.

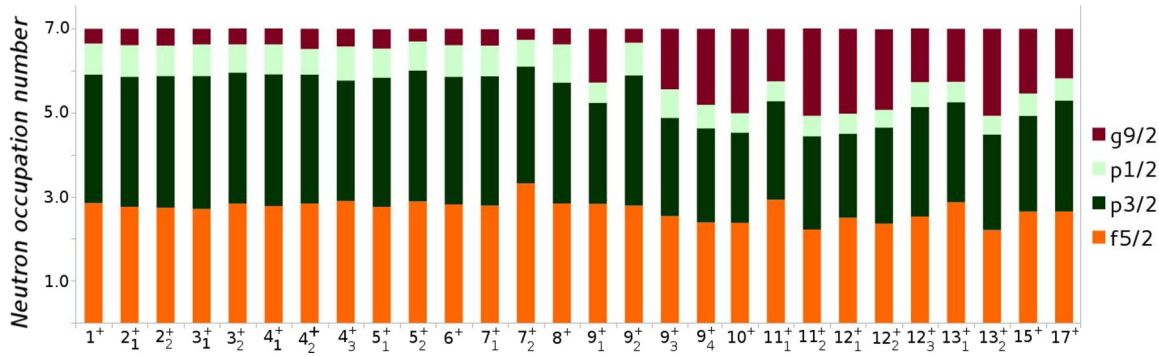

FIG. 11. Calculated occupation probabilities of the $f_{5/2}$, $p_{3/2}$, $p_{1/2}$, and $g_{9/2}$ orbitals for the positive parity states for neutrons in ^{66}Ga. The occupation probabilities are calculated from the shell model using the jun45pn interaction. Please see text for details.

interaction, whereas the first 14^- state is underpredicted by 271 keV in energy. The main configuration of the first excited 14^- state, as predicted by the jun45pn interaction, is $[\pi(p_{3/2})^2(g_{9/2})^1]_{j_p=9/2} \otimes [\nu(f_{5/2})^3(p_{3/2})^2(g_{9/2})^2]_{j_\nu=19/2}$ and that of second excited 14^- state is $[\pi(f_{5/2})^1(p_{3/2})^2]_{j_p=9/2} \otimes [\nu(f_{5/2})^3(p_{3/2})^3(g_{9/2})^1]_{j_\nu=19/2}$. So, for the first excited 14^- state, contributions of $g_{9/2}$ orbitals for both protons and neutrons are significantly large with respect to the second 14^- state, and this is also obvious from the occupation number (calculated using the jun45pn interaction) plot (Fig. 13). The energy of the 16^- state is in moderate agreement with the jj44bpn calculation but is well underpredicted by jun45pn. The configuration of this state is mainly originating from protons and neutrons in the $f_{5/2}$, $p_{3/2}$, and $g_{9/2}$ orbitals. The occupation number plots (Figs. 8–13) also suggest that, for both kinds of interaction, the contributions coming from both protons and neutrons in the $g_{9/2}$ orbitals are significantly large for high spin positive and negative parity states. Hence, a variety of structural effects are expected due to the occupancy of the shape driving $g_{9/2}$ orbitals. The low spin positive parity states up to 4^+ are mainly due to the occupation of protons in the $p_{3/2}$ orbital, and those above are due to protons in the $f_{5/2}$ and $p_{3/2}$ orbitals up to spin value $\approx 8\hbar$, as obtained from the calculations using the jun45pn interaction. Significant contributions in wave functions for low spin positive parity states up to 8^+ originate from neutrons occupying the $f_{5/2}$ and $p_{3/2}$ orbitals. For high spin positive (13^+ to 17^+) and negative (14^- and 16^-) parity states, angular momenta are mainly generated by the $(\pi f_{5/2}p_{3/2}g_{9/2})^3 \otimes (\nu f_{5/2}p_{3/2}g_{9/2})^7$ configuration, as predicted by both interactions. It is also evident from the calculations with both interactions that the participation of the $p_{1/2}$ orbital for the generation of both low and high angular momentum states is insignificant.

V. CONCLUSION

A new level scheme of ^{66}Ga has been proposed in this present work, which is enriched with 21 new transitions and 20 new levels. Some of the previously observed states, without any definite spin-parities, are assigned with definite or tentative values in this work, from the measured values of DCO ratio and polarization asymmetry of depopulating transitions. Multipolarities of many new transitions are determined from the measurements. The level scheme has been extended up to $\approx$11.6 MeV in energy. Some intermediate spin states of ^{66}Ga are explained in the framework of coupling of single-particle configurations with the vibrational core. Shell model calculations have also been performed in $f_{5/2}pg_{9/2}$ model space using two different interactions, viz., jj44bpn and jun45pn. Comparative study shows that the jun45pn interaction is more efficient in explaining the lower excitations than jj44bpn. Both interactions are in moderate agreement in explaining intermediate spin states. With an improved set of the two-body matrix elements and incorporating the full $fpg_{9/2}$ model space, i.e., including the $1f_{7/2}$ orbital for calculations, a more accurate description may be obtained. High spin states above 15^+ are observed to be different from the single-particle nature, and it is probably the collective degrees of freedom that come into play at such high spin. More experimental investigation is required to confirm the nature of the collectivity at such high spin.

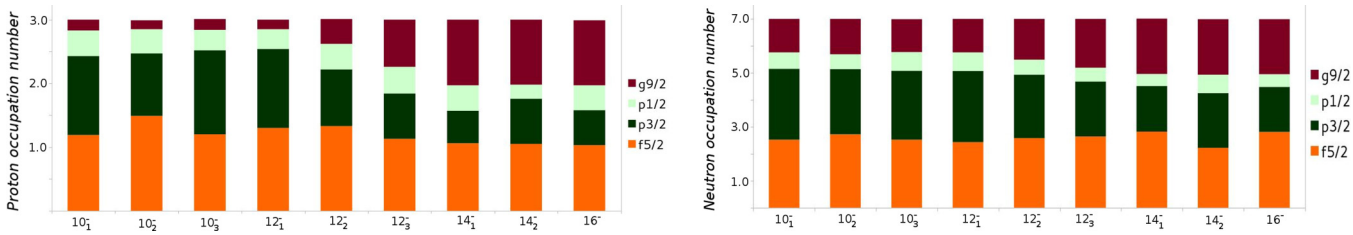

FIG. 12. Calculated occupation probabilities of the $f_{5/2}$, $p_{3/2}$, $p_{1/2}$, and $g_{9/2}$ orbitals for the negative parity states for protons and neutrons in ^{66}Ga. The occupation probabilities are calculated from the shell model using the jj44bpn interaction. Please see text for details.

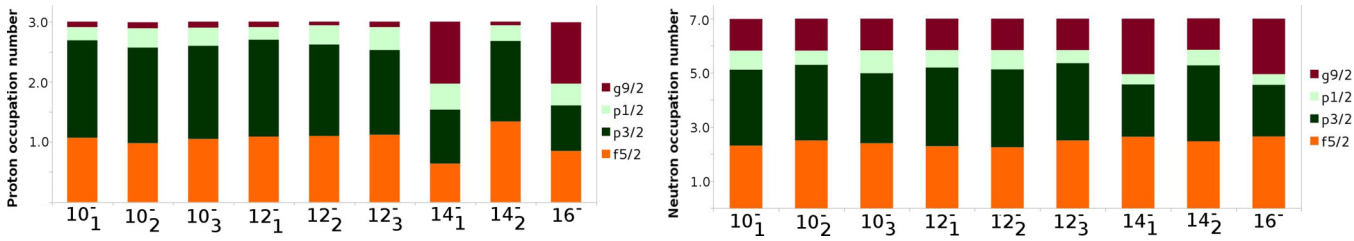

FIG. 13. Calculated occupation probabilities of the $f_{5/2}$, $p_{3/2}$, $p_{1/2}$, and $g_{9/2}$ orbitals for the negative parity states for protons and neutrons in ^{66}Ga. The occupation probabilities are calculated from the shell model using the jun45pn interaction. Please see text for details.

ACKNOWLEDGMENTS

We would like to acknowledge the Pelletron staff of IUAC for providing excellent beams and INGA collaborators for the loan of detectors. Support from the target laboratory and from D. Kanjilal, IUAC is gratefully acknowledged. We would like to thank S. Nandi (VECC), S. S. Bhattacharjee (TRIUMF, Canada), and R. Garg (IUAC) for their help during the experiment. We would also like to acknowledge financial support from SERB/DST (New Delhi), file No. EMR/2015/000891, IUAC (New Delhi), file No. UFR49318 and DAE-BRNS, Project Sanction No. 37(3)/14/17/2016-BRNS.

[1] C. E. Svensson *et al.*, Phys. Rev. Lett. **82**, 3400 (1999).
[2] L.-L. Andersson *et al.*, Phys. Rev. C **79**, 024312 (2009).
[3] C. E. Svensson *et al.*, Phys. Rev. Lett. **79**, 1233 (1997).
[4] C. E. Svensson *et al.*, Phys. Rev. Lett. **80**, 2558 (1998).
[5] U. S. Ghosh *et al.*, Phys. Rev. C **100**, 034314 (2019).
[6] A. K. Singh *et al.*, Phys. Rev. C **57**, 1617 (1998).
[7] D. Karlgren *et al.*, Phys. Rev. C **69**, 034330 (2004).
[8] B. Mukherjee, S. Muralithar, R. P. Singh, R. Kumar, K. Rani, R. K. Bhowmik, and S. C. Pancholi, Phys. Rev. C **64**, 024304 (2001).
[9] M. Weiszflog *et al.*, Eur. Phys. J. A **11**, 25 (2001).
[10] S. S. Bhattacharjee *et al.*, Phys. Rev. C **95**, 054330 (2017).
[11] I. Dankó *et al.*, Phys. Rev. C **59**, 1956 (1999).
[12] A. K. Singh *et al.*, Eur. Phys. J. A **9**, 197 (2000).
[13] D. Ward *et al.*, Phys. Rev. C **63**, 014301 (2000).
[14] E. A. Stefanova *et al.*, Phys. Rev. C **67**, 054319 (2003).
[15] L. Cleemann *et al.*, Nucl. Phys. A **386**, 367 (1982).
[16] H. H. Bolotin and D. A. McClure, Phys. Rev. **180**, 987 (1969).
[17] C. Morand, M. Agard, J. F. Bruandet, A. Dauchy, A. Giorni, F. Glasser, and T. U. Chan, Nucl. Phy. A **308**, 103 (1978).
[18] C. C. Lu, M. S. Zisman, and B. G. Harvey, Phys. Rev. **186**, 1086 (1969).
[19] J. Timár, T. X. Quang, T. Fényes, Z. Dombrádi, A. Krasznahorkay, J. Kumpulainen, R. Julin, S. Brant, V. Paar, and L. Šimičič, Nucl. Phys. A **573**, 61 (1994).
[20] M. R. Najam, W. F. Davidson, W. M. Zuk, L. E. Carlson, and M. A. Awal, Nucl. Phys. A **173**, 577 (1971).
[21] R. A. Hinrichs, R. Sherr, G. M. Crawley, and I. Proctor, Phys. Rev. Lett. **25**, 829 (1970).
[22] http://www.nndc.bnl.gov.
[23] A. Filevich, A. Ceballos, M. A. J. Mariscotti, P. Thieberger, and E. D. Mateosian, Nucl. Phys. A **295**, 513 (1978).
[24] G. K. Mehta *et al.*, Nucl. Instrum. Methods Phys. Res. A **268**, 334 (1988).
[25] S. Muralithar *et al.*, Nucl. Instrum. Methods Phys. Res. A **622**, 281 (2010).
[26] B. P. Ajith Kumar *et al.*, in *Proceedings of the 44th DAE-BRNS Symposium on Nuclear Physics* (Department of Atomic Energy, Government of India, Mumbai, 2001), p. 390.
[27] D. C. Radford, Nucl. Instrum. Methods Phys. Res., Sect. A **361**, 297 (1995).
[28] R. K. Bhowmik *et al.*, in *Proceedings of the 44th DAE-BRNS Symposium on Nuclear Physics* (Department of Atomic Energy, Government of India, Mumbai, 2001), p. 422.
[29] S. Rai *et al.*, Eur. Phys. J. A **54**, 84 (2018).
[30] K. S. Krane *et al.*, Nucl. Data Tables **11**, 351 (1973).
[31] G. Duchene *et al.*, Nucl. Instrum. Methods Phys. Res. A **432**, 90 (1999).
[32] K. Starosta *et al.*, Nucl. Instrum. Methods Phys. Res. A **423**, 16 (1999).
[33] F. W. N. de Boer *et al.*, Nucl. Phys. A **158**, 166 (1970).
[34] E. A. McCutchan *et al.*, Nucl. Data Sheets **113**, 1735 (2012).
[35] M. Honma, T. Otsuka, T. Mizusaki, and M. Hjorth-Jensen, Phys. Rev. C **80**, 064323 (2009).
[36] A. F. Lisetskiy, B. A. Brown, M. Horoi, and H. Grawe, Phys. Rev. C **70**, 044314 (2004).
[37] A. Brown and W. D. M. Rae, Nucl. Data Sheets **120**, 115 (2014).
[38] S. Rai *et al.*, Int. J. Mod. Phys. E **25**, 1650099 (2016).